Available online at www.sciencedirect.com
SCIENCE DIRECT®
Remote Sensing of Environment 103 (2006) 419–437
Remote Sensing of Environment
www.elsevier.com/locate/rse

Detecting the red tide algal blooms from satellite ocean color observations in optically complex Northeast-Asia Coastal waters

Yu-Hwan Ahn, Palanisamy Shanmugam *

Ocean Satellite Research Group, Korea Ocean Research and Development Institute (KORDI), Ansan P.O. Box 29, Seoul 425-600, Korea

Received 18 January 2006; received in revised form 13 April 2006; accepted 19 April 2006

Abstract

Over the last few decades, the coastal regions throughout the world have experienced incidences of algal blooms, which are harmful or otherwise toxic because of their potential threat to humans as well as marine organisms, owing to accelerated eutrophication from human activities and certain oceanic processes. Previous studies have found that correct identification of these blooms remains a great challenge with the standard bio-optical algorithms applied to satellite ocean color data in optically complex coastal waters containing high concentrations of the interfered dissolved organic and particulate inorganic materials. Here a new method called the red tide index (RI) is presented which is capable of identifying potential areas of harmful algal blooms (HABs) from SeaWiFS ocean color measurements representing the typical Case-2 water environments off the Korean and Chinese coasts. The RI method employs the water-leaving radiances (L_w), collected from in-situ radiometric measurements of three SeaWiFS bands centered at 443 nm, 510 nm and 555 nm, to achieve derivation of indices that are then related to absorbing characteristics of harmful algae (i.e., L_w at 443 nm) from which a best fit with a cubic polynomial function with correlation coefficient of $R^2=0.91$ is obtained providing indices of higher ranges for HABs and lower and slightly reduced ranges for turbid and non-bloom waters. Similar indices derived from the use of remote sensing reflectance (R_{rs}), normalized water-leaving radiance (nL_w) and combination of both are found rather inadequate to characterize the variability of the encountered bloom. In order to quantify the HABs in terms of chlorophyll (Chl), an empirical relationship is established between the RI and in-situ Chl in surface waters from about 0.4–71 mg m^{-3}, which yields a Red tide index Chlorophyll Algorithm (RCA) based on an exponential function with correlation coefficient $R^2=0.92$. The established methods were extensively tested and compared with the performances of standard Ocean Chlorophyll 4 (OC4) algorithm and Local Chlorophyll Algorithm (LCA) using SeaWiFS images collected from typical red tide waters of Korean South Sea (KSS), East China Sea (ECS), Yellow Sea (YS) and Bohai Sea (BS) during 1999–2002. The standard spectral ratio algorithms, the OC4 and LCA, yielded large errors in Chl retrievals for coastal areas, besides providing false information about the encountered HABs in KSS, ECS, YS and BS waters. On the contrary, the RI coupled with the standard spectral ratios yielded comprehensive information about various ranges of algal blooms, while RCA Chl showing a good agreement with in-situ data led to enhanced understanding of the spatial and temporal variability of the recent HAB occurrences in high scattering and absorbing waters off the Korean and Chinese coasts.

Keywords: Satellite ocean color; HABs; Red tide Index; Red tide index Chlorophyll Algorithm; OC4 bio-optical algorithm; SeaWiFS; Korea

1. Introduction

Harmful algal blooms (HABs) (also termed as red tides) have been found to occur frequently in optically complex Case-2 waters of the Korean South Sea (KSS) (Ahn et al., 2006; Kim et al., 1990), and neighboring waters of East China Sea (ECS) (Chen et al., 2003; Gao & Song, 2005), Yellow Sea (YS) (Ahn et al., 2004), Bohai Sea (BS) (Tang et al., 2006) and Japanese Sea (JS) (Yuki & Yoshimatsu, 1989; Fukuyo et al., 1990). These blooms are dominated mostly by *Cochlodinium polykrikoides* (hereafter referred to as *C. polykrikoides), Alexandrium tamarense*, *Prorocentrum dentatum* and *Ceratium furca,* causing massive mortalities of aquaculture fish and numerous ecological and health impacts since the last few decades. In the KSS, Kim (1998) have

* Corresponding author. Tel.: +82 31 400 7607; fax: +82 31 400 7606.
E-mail addresses: pshanmugam@kordi.re.kr, pshanmugam90@hotmail.com (P. Shanmugam).

0034-4257/$ - see front matter © 2006 Elsevier Inc. All rights reserved.
doi:10.1016/j.rse.2006.04.007

documented several *C. polykrikoides* bloom events along with an extensive event in summer 1995, which caused heavy mortalities of aquaculture fish amounting to a loss of ~ US$ 95.5 million. It was already reported from South China Sea during March and April 1998 that HABs appear to have caused tremendous damage to the coastal aquaculture industry, wiping out 1500 tonnes of farmed fish, which was equivalent to half of the entire Hong Kong aquacultural production of 1997 (Anderson, 1998; Tang et al., 2003). A recent report showed evidence of *C. furca* that dominated a 5000 km^2 area of the Bohai Sea during summer, causing an economic loss amounting to about 62 million US$ (EQB, 2000). Enhanced anthropogenic nutrification as one of the most pervasive changes altering coastal environments and a steepening of the nutricline by intervening physical phenomena offshore were suggested to be the main causes of frequent and spatially widespread HABs responsible for deteriorating the health of the ecosystem of the coastal and oceanic environment (Burkholder, 1998; Falkowski et al., 1991; Olaizola et al., 1993; Shumway, 1990). Though non-HAB species are stimulated proportionally, a modest increase in the abundance of a HAB species can cause it to become noticeable because of its toxic or harmful effects (Anderson et al., 2002).

In order to mitigate the impacts of HABs, it is therefore very essential to detect, monitor and forecast their development and movement using currently available remote sensing technology because traditional ship-based field sampling and analysis are very limited in both space and temporal frequency. Major satellite ocean color sensors, such as Sea-viewing Wide Field-of-view Sensor (SeaWiFS), can be ideal instruments for estimating global phytoplankton biomass, especially in episodic blooms, because they provide relatively high frequency synoptic information over large areas (Hooker & McClain, 2000). They measure upwelled radiance for several narrow bands in the visible to near-infrared (NIR) spectral range specifically determined for the study of the properties of various colored constituents in the surface ocean, including phytoplankton, detritus, colored dissolved organic matter (DOM) and suspended sediments (SSC). With these bands and adequate spatial resolution it may be possible to detect and trace HABs such as *C. polykrikoides* and *A. tamarense* and *C. furca* from space because their population is maximum at near surface waters (0–15 m). This produces the magnitude of water-leaving radiances at blue wavelength (443 nm) to be lower than other phytoplankton (like diatom) due to their higher chlorophyll-specific absorption, and the water-leaving radiance at green wavelength (555 nm) to be higher than other phytoplankton due to the influence of strong pigment backscattering (Ahn & Moon, 1999; Ahn et al., 2006).

Satellite detection and monitoring of HABs require methods/algorithms that have been developed mostly based on extensive in-situ bio-optical observations from optically less complex oceanic waters and optical modelling of water properties. Steidinger and Haddad (1981) were among the first to make use of the chlorophyll (Chl) bio-optical algorithm developed for Coastal Zone Color Scanner (CZCS) for detection of *Karenia brevis* bloom in western Florida-Shelf waters. When SeaWiFS became operational, several studies appeared to have focused their efforts to exploit usefulness of satellite-derived Chl data to delineate the potential areas of *K. brevis* blooms in the waters of Gulf of Mexico, *Gymnodinium catenatum* blooms in the waters of New Zealand and South China Sea and *A. tamarense* blooms in the waters of East China Sea (Chang et al., 2001; Chen et al., 2003; Tang et al., 2003; Stumpf, 2001). The routine monitoring has been initiated based on chlorophyll anomalies obtained from SeaWiFS image, which have served as indices of potential *K. brevis* blooms in the Gulf of Mexico (Tomlinson et al., 2004). However, accurate detection of HABs based on these data seemed to be ineffective because of the absence of contemporaneous observations of the documented blooms by satellites. Moreover, satellite-derived Chl concentrations most likely suffer from uncertainties in inappropriate atmospheric correction, interference of coastally influenced colored dissolved organic and particulate inorganic components and perhaps even a shallow bottom (Darecki & Stramski, 2004).

High chlorophyll anomaly is not always necessarily due to harmful blooms because other non-HAB species can often exhibit similar pigment concentrations. On the other hand, the cases of less photosynthetic red tide organisms may produce weaker chlorophyll signature that cannot be captured from the satellite-derived Chl anomalous image (Cokacar et al., 2004). Therefore, delineation of a particular phytoplankton species was accomplished with the development of robust techniques based on unique optical properties of harmful algae (Brown & Yoder, 1994; Subramaniam & Carpenter, 1994). Cannizzaro et al. (2002) determined *K. brevis* has lower backscatter property than blooms of other diatom and dinoflagellate species and recently they proposed new algorithms based on in-situ data to use the backscattering/Chl ratio to differentiate HABs from other non-HABs. However, operational use of these methods would be successful only in waters with less abundance in dissolved organic and particulate inorganic matters. Studies have also involved evaluating the classical spectral enhancement and classification techniques to delineate the areas of HABs from other optical water types. For instance, Pasterkamp et al. (2002) and Danaher and Omongain (1992) established algal bloom classes from satellite data using supervised classification techniques, while Ahn et al. (2006) explored potential use of Forward Principal Component Analysis (FPCA) and Minimum Spectral Distance (MSD) classification methods in order to detect the blooms of *C. polykrikoides* in Korean waters. Though accurate atmospheric correction is not required for these methods, the success predominantly depends on the knowledge of the study area, prototypical data points used to train the methods and optical significance of various water features.

To overcome the limitations and problems associated with the above methods, recent studies needed to look for other methods based on fluorescence line height (FLH) measurements estimated using band triplets included in the Medium Resolution Imaging Spectrometer (MERIS) and Moderate resolution Imaging Spectrometer (MODIS) sensors. Ahn and Shanmugam (in press) observed an apparent increase in the magnitude of FLH when Chl concentration of red tide waters increased and the position of fluorescence peak remained stable at around 685. They suggested that estimation of FLH from satellite ocean color data could improve the accuracy of detecting and tracing HABs particularly in coastal areas where it requires simple atmospheric correction rather than complex methods based on modelling and characterizing aerosol and atmospheric properties. One recent study showed that the patterns of HABs inferred from satellite MODIS FLH data were consistent with concurrent in-situ observations in the South West Florida coastal waters where the traditional band ratio algorithm yielded false information about the blooms (Hu et al., 2005). However, the success of this approach may suffer from significant variations in Chl fluorescence efficiency depending on availability of nutrients, light intensity, temperature and physiological aspects of phytoplankton (Babin et al., 1996). Furthermore, in Case-2 waters weak Chl fluorescence emerges at the surface after complex interactions with suspended particulate materials through the turbid water column (Ahn & Shanmugam, in press; Babin et al., 1996). Thus, correct identification of HABs from non-HAB and turbid waters remains uncertain with this data.

Thus, the main objectives of this research are as follows: (1) development and application of Red tide Index (RI)and Red tide index Chlorophyll Algorithm (RCA) for correct identification of HABs from satellite ocean color measurements in optically complex Case-2 water environments off the Korean and Chinese coasts, (2) extension of RI to delineate the patches of other phytoplankton blooms around coastal areas of the ECS, BS and YS, (3) assessment of the applicability of standard spectral ratios bio-optical algorithms for detecting HABs in these waters, and (4) validation of the presented methods using in-situ data and addressing the sources of error that limit the potential utility of satellite ocean color data for this application.

2. Materials and methods

2.1. Characteristics of the considered Case-2 water environments

Fig. 1 illustrates the characteristics of complex Case-2 water environments of the KSS, YS, ECS and BS determined by major physical currents such as the Kuroshio Warm Current

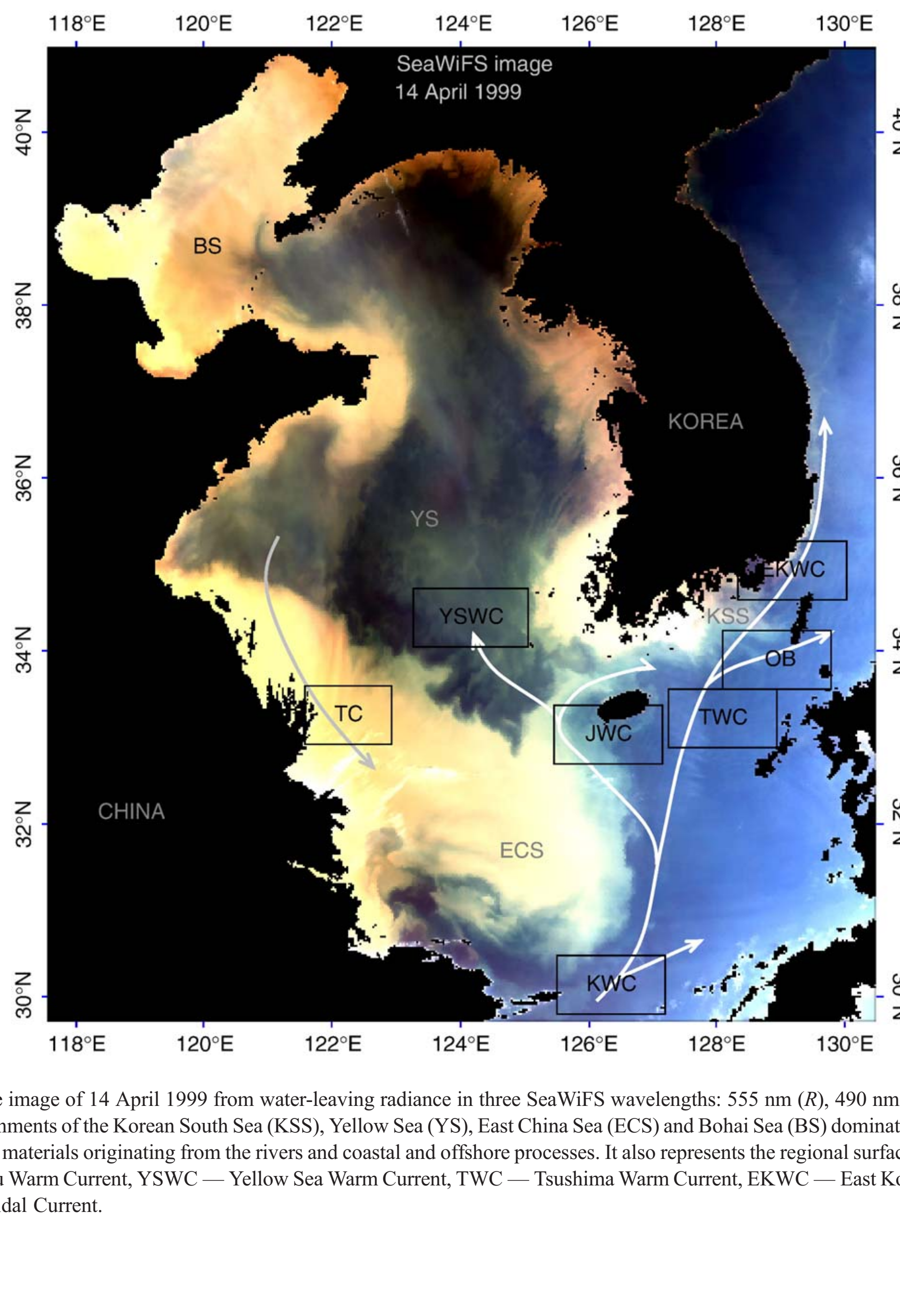

Fig. 1. The color composite image of 14 April 1999 from water-leaving radiance in three SeaWiFS wavelengths: 555 nm (*R*), 490 nm (*G*) and 412 nm (*B*), showing typical Case-2 water environments of the Korean South Sea (KSS), Yellow Sea (YS), East China Sea (ECS) and Bohai Sea (BS) dominated by very high concentrations of dissolved and particulate materials originating from the rivers and coastal and offshore processes. It also represents the regional surface currents: KWC — Kuroshio Warm Current, JWC — Jeju Warm Current, YSWC — Yellow Sea Warm Current, TWC — Tsushima Warm Current, EKWC — East Korea Warm Current, and OB — Offshore Branch, TC — Tidal Current.

(KWC) and its branches, the Tsushima Warm Current (TWC) and Jeju Warm Current (JWC), and sub-branches the East Korean Warm Current (EKWC) along the Korean east coast and Offshore Branch (OB) along the Japanese coast (Chang et al., 2002; Lie et al., 1998). The concentrations of Chl in the surface waters of KSS normally range from 0.2 to 72 mg m^{-3} (occasionally reaching over 100 mg m^{-3}), suspended sediments (SSC) from 0.5 to 125 g m^{-3} and dissolved organic matter (DOM) from 0.2 to 2 m^{-1} (Ahn et al., 2001). The most dominant species of HABs of this region is a highly toxic dionoflagellate *C. polykrikoides* which occurs particularly during summer and fall seasons with concentrations ranging from 1×10^3 cells ml^{-1}–3×10^4 cells ml^{-1} (Kim, 1990; Ahn et al., 2006).

In the ECS the 6300 km long Yangtze river drains a catchment area of 1.96×10^6 km^2 in China with annual discharge of 9.8×10^{11} m^3, exporting abundant quantities of nutrients (annual fluxes of total inorganic nitrogen, phosphate, silicate and nitrate are 8.88×10^6 t, 1.36×10^4 t, 2.04×10^6 t and 6.36×10^6 t respectively) and sediments (annual sediment load is 4.86×10^8 t with an average SSC level of about 500 mg l^{-1}) to the estuary and areas in its vicinity (Gao & Song, 2005; Shen et al., 1992). The sedimentation and resuspension processes at the same time are intense due to strong tidal amplitude (an average of 4.5–5.0 m) and current (2.0–2.5 m s^{-1}) around the estuary (Huang, 1992). *P. dentatum* and *Noctiluca scintillans* and *A. tamarense* were reported to be the main red tide causative agents in the vicinity of the estuary and its offshore waters (Chen et al., 2003; Hong, 2003). They are generally non-toxic but can be harmful by choking the gills or having other effects due to depletion of dissolved oxygen in water, leading to massive fish kills and other important species mortalities (Chen et al., 2003; Gao & Song, 2005).

The spring YS water mass, characterized by the high temperature and high salinity Yellow Sea Warm Current (YSWC), the high nutrient Yellow Sea Cold Water (YSCW), the low temperature and low salinity Coastal Current Water (CCW) and the low salinity Yangtze River Diluted Water (YRDW), is stirred in a large scale (Hyun & Kim, 2003) which provides favorable conditions for the massive dinoflagellate *A. tamarense* and *Prorocentrum compressum* blooms in the YS offshore domain and for diatom *Skeletonema coastatum* and *Paralia sulcata* blooms in the YS coastal areas.

The BS is relatively shallow (an average 18 m depth) and the largest inner sea of China with a total area of 77,000 km^2. Of the 17 rivers that discharge into the BS, the Yellow River is the most dominant because of its huge discharge of 420×10^8 m^3 $year^{-1}$, sediment load (10×10^8 t $year^{-1}$), nutrients quantities in the following amounts — 71.18 kt $year^{-1}$ NO_3–N and 0.43 kt $year^{-1}$ PO_4–P (Zhang et al., 1994). The Chl concentration is elevated in spring and summer from 0.2 up to 7.5 mg m^{-3}. *C. furca*, a typical dinoflagellate, was reported to cause massive economic damage to the BS (EQB, 2000). Diatom blooms often dominate the BS during spring and autumn (Wei et al., 2004).

2.2. In-situ bio-optical data assimilation

The bio-optical data collected from a wide range of waters were used in the derivation of red tide index (RI) algorithm for identifying HABs in the surface waters of the KSS, YS and ECS. In-situ bio-optical measurements were performed during several cruises conducted in the Korean seas and neighboring waters through the years 1998–2004 onboard the research vessels EARDO, Olympic and Tamgu (Table 1). Of these, six cruises coincided with the rapid growth and initiation of *C. polykrikoides* blooms in the KSS (particularly around the Jinhae bay and off the Geoje Island) during August 1998–2004. During each cruise, the water samples were collected with buckets/Niskin bottles and sub samples were filtered onboard onto Whatman GF/F glass microfiber filters for measurement of

Table 1
In-situ data collected from Korean seas and neighboring waters

Observation area	Parameters observed	No of data	Date
Bay of Jin-hae and around area of Geoje island (KSS east)	L_w, R_{rs}, nL_w, Chl, SSC, DOM, a_p, a_{ss}	18	Aug. 26–28, 1998
Around area of Geoje island and Jeju strait (KSS west)	L_w, R_{rs}, nL_w, Chl, SSC, DOM, a_p, a_{ss}	33	Sep. 23–26, 1998
Around area of Jindo and Wando (KSS west)	L_w, R_{rs}, nL_w, Chl, SSC, DOM	58	Oct. 20–23, 1998
Bay of Jin-hae and around area of Geoje island (KSS east)	L_w, R_{rs}, nL_w, Chl, SSC, DOM, a_p, a_{ss}	32	Aug. 9–10, 1999
Around area of Wando KSS west)	L_w, R_{rs}, nL_w, Chl, SSC, DOM, a_p, a_{ss}	5	Sep. 2–3, 1999
East Sea (ES)	L_w, R_{rs}, nL_w, Chl, SSC, DOM, a_p, a_{ss}	30	May 19–29, 2000
Jeju strait (KSS west)	L_w, R_{rs}, nL_w, Chl, SSC, DOM, a_p, a_{ss}	22	July 21–23, 2000
Southern area of Yellow Sea (YS)	L_w, R_{rs}, nL_w, Chl, SSC, DOM, a_p, a_{ss}	15	Feb. 1–5, 2001
Yellow Sea (YS)	L_w, R_{rs}, nL_w, Chl, SSC, DOM	20	June 4–15, 2001
Bay of Jin-hae and coastal area of the South Sea (KSS east)	L_w, R_{rs}, nL_w, Chl, SSC, DOM, a_p, a_{ss}	32	Aug. 28–31, 2001
Southern area of Yellow Sea (YS)	L_w, R_{rs}, nL_w, Chl, SSC, DOM, a_p, a_{ss}	5	Dec. 5–20, 2001
East China Sea (ECS)	L_w, R_{rs}, nL_w, Chl, SSC, DOM, a_p, a_{ss}	20	Feb. 19–25, 2002
Southern area of Yellow Sea YS)	L_w, R_{rs}, nL_w, Chl, SSC, DOM, a_p, a_{ss}	7	May 2–3, 2002
South Sea and Southern west area of Jeju (KSS west)	L_w, R_{rs}, nL_w, Chl, SSC, DOM, a_p, a_{ss}	21	June 18–22, 2002
Around area of Geoje island and coastal area of the South Sea (KSS east)	L_w, R_{rs}, nL_w, Chl, SSC, DOM, a_p, a_{ss}	26	Sep. 2–7, 2002
Southern area of Yellow Sea (YS)	L_w, R_{rs}, nL_w, Chl, SSC, DOM, a_p, a_{ss}	71	Feb. 9–18, 2003
Bay of Jin-hae and around area of Geoje island (KSS east)	L_w, R_{rs}, nL_w, Chl, SSC, DOM, a_p, a_{ss}	26	Aug. 5–6, 2003
East China Sea (ECS)	L_w, R_{rs}, nL_w, Chl, SSC, DOM, a_p, a_{ss}	10	Oct. 8–10, 2003
East China Sea (ECS)	L_w, R_{rs}, nL_w, Chl, SSC, DOM, a_p, a_{ss}	11	March 23–25, 2004
Yellow Sea (YS)	L_w, R_{rs}, nL_w, Chl, SSC, DOM, a_p, a_{ss}	12	May 9–12, 2004

chlorophyll (chl), suspended sediments (SSC) and phytoplankton absorption ($a_{ph}(\lambda)$). These filters were frozen at dark conditions until analysis took place at the laboratory with the standard spectrophotometric method for determining Chl and a_{ph} and oven-drying method for SSC (Ahn et al., 2001; Kishino et al., 1984; Lee et al., 1998). DOM absorption spectra were obtained from spectrophotometric method. Simultaneously, radiometric measurements such as downward spectral irradiance (E_d (λ)) and total water-leaving radiance ($tL_w(\lambda)$) and sky radiance (L_{sky} (λ)) were performed at various sample sites using an ASD FieldSpec Pro Dual VNIR Spectroradiometer with spectral range from 350–1050 nm and spectral sample interval of 1.4 nm. This instrument was calibrated every year and several inter-calibrations with other instruments were performed to confirm its stability. Most of these measurements were generally made in excellent conditions, near solar noon and under almost cloudless conditions. The data recorded in units of mW cm^{-2} μm^{-1} sr^{-1} needed to be corrected for the contribution of skylight reflection and air–sea interface effects (Ahn et al., 2001). Thus, the measured total water-leaving radiance (tL_w (λ)) was corrected for the sky light reflection and the air–sea interface effects using the following equation,

$$L_w(\lambda) = tL_w(\lambda) - F_r(\lambda) \times L_{sky}(\lambda) \tag{1}$$

The values of $L_{sky}(\lambda)$ were obtained from the sky radiometer and F_r value was assumed to be constant 0.025 (Austin, 1974). In fact, F_r varies with viewing geometry, sky conditions (clear, partially and densely cloudy) and sea surface roughness due to wind and is wavelength-dependent under a cloudy sky (Mobley, 1999). The remote sensing reflectance ($R_{rs}(\lambda)$) was obtained by normalizing the corrected water-leaving radiance ($L_w(\lambda)$) to spectral downwelling irradiance (E_d) as follows,

$$R_{rs}(0^+\lambda) = \frac{L_w(\lambda)}{E_d(0^+\lambda)} \tag{2}$$

The $R_{rs}(\lambda)$ can also be obtained by using L_w=0.54 L_u (0^-), and E_d (0^-)=0.96 E_d (0^+), where 0.54 is a mean coefficient summarizing the effect of internal reflection of the upwelling radiance flux during transmission through the interface, and 0.96 accounts for the loss of the downwelling flux by reflection at the air–sea interface (Austin, 1974; Morel & Antoine, 1994). From remote sensing reflectance the normalized water-leaving radiance (nL_w) may be obtained (as the water-leaving radiance can be changed with light field conditions of surface layer of the ocean) using the following relation

$$nL_w(\lambda) = L_w(\lambda)\frac{F_0(\lambda)}{E_d(\lambda)} \tag{3}$$

where F_0 is the mean extraterrestrial solar irradiance at a given spectral band.

In addition to the above data, for validating the results of developed methods Chl, SSC, nutrients (NO_3^-N, PO_4^-P, SiO_2^-Si), salinity and temperature data for YS and cell count data of *C. polykrikoides* for KSS were obtained from the National Fisheries Research and Development Institute (NFRDI). These data were collected on the ship from a number of oceanographic stations established by NFRDI under the support of Ministry of Maritime Affairs and Fisheries (MOMAF).

2.3. Satellite data and image processing

SeaWiFS ocean color images of spring and summer from 1999–2002 were acquired using the High Resolution Picture Transmission (HRPT) antenna located at Korea Ocean Research and Development Institute (KORDI). SeaWiFS ocean color instrument flown on Orbview-2, the SeaStar satellite in August 1997 by NASA, was specifically designed to provide near-global coverage every 2 days of upwelled radiance for eight narrow spectral channels (nm) in the visible and near-infrared spectral range (402–422, 433–453, 480–500, 500–520, 545–565, 660–680, 745–785, and 845–885) with the spatial resolution of ~ 1 km/pixel at nadir (Hooker et al., 1994). The radiances recorded at the top of the atmosphere (TOA) were atmospherically corrected and processed to level 2 using NASA SeaDAS version 4.4 (Tomlinson et al., 2004). The surface Chl concentrations were then estimated by using NASA Ocean Chlorophyll 4 (OC4) bio-optical algorithm within SeaDAS software. The SeaWiFS OC4 algorithm is a maximum band ratio algorithm employing 4 spectral bands: band 2, 3, 4 and 5. Band 5 (555 nm) is taken as the reference wavelength band and three band ratios are computed for each measurement of the radiance or reflectance spectrum as given in O'Reilly et al. (1998):

$$\langle Chl \rangle = 10^{0.366-3.067R+1.930R^2+0.649R^3-1.532R^4} \quad \text{where } R = \log_{10}\left\{\frac{R_{rs}(443)>R_{rs}(490)>R_{rs}(510)}{R_{rs}(555)}\right\} \tag{4}$$

and R_{rs} is the remote sensing reflectance. The OC4 algorithm is purely empirical in that it applies simple regression between the field determinations of pigment concentration and spectral ratios of ocean reflectance or normalized water-leaving radiance. The OC4 algorithm has been considered as standard method for satellite detection of HABs over the global waters (Cokacar et al., 2004; Stumpf, 2001; Tang et al., 2003; Tomlinson et al., 2004).

2.4. Background of Red tide Index (RI) method

The red tide index (RI) hypothetically differs from the standard spectral ratios algorithms that are sensitive not only to Chl but also to other water constituents such as SSC and DOM. RI are achieved based on the principle that rapid growth of red tide organisms absorbs radiation in the lower green to blue wavelength part of spectrum while strongly reflecting radiation in the green wavelength part of the spectrum. Here instead of taking the direct radiance ratio between the blue and green wavelengths, RI is built by normalizing the deducted and combined ratio $L_w(510)/L_w$ (555) nm with the absolute values of water-leaving radiance at 443 nm as follows,

$$RI = \frac{[L_w(510)/L_w(555) - L_w(443)]}{[L_w(510)/L_w(555) + L_w(443)]} \tag{5}$$

This allows a good separation of red tides from other dominant optical types. RI values vary from −1 to +1. A red tide index value of −1 means absence of harmful algal bloom (HAB) and close to +1 indicates the highest possible of HABs. For deep blue waters with less phytoplankton and other agents such as nanophytoplankton and heterotrophic bacteria and viruses and waters with substances other than phytoplankton such as suspended inorganic particles (SSC) and dissolved organic matter (DOM) (and perhaps even a bottom reflectance) that make a significant contribution to the optical properties of the coastal waters (Ahn et al., 2001; Arnone et al., 2004; Sathyendranath, 2000), the red tide indices decrease progressively and are often <0.0. The idea behind derivation of RI came from earlier demonstrations showing how three bands separate red tides from turbid and non-bloom waters off the Korean coast (Ahn et al., 2006). The above expression is more appropriate for measurements of near noon time, but can be easily adopted with the quantities of normalized water-leaving radiance (nL_w) that are generally independent of time of the measurements. Sections 3.1 and 3.2 evaluate the use of this quantity for red tide detection using ocean color measurements of near noon time.

In order to derive the red tide indices, the digital counts of Level 1A SeaWiFS raw data product obtained from KORDI HRPT station were converted to total radiance (mW cm^{-2} μm^{-1} sr^{-1}) at the level of the top of the atmosphere (TOA) by employing the SeaWiFS band sensitivity and pre-launch calibration coefficients given in NASA's SeaWiFS technical report series (Hooker et al., 1994). This was followed by the performance of atmospheric correction with Spectral Shape Matching Method (SSMM) developed by Ahn and Shanmugam (2004). This method of atmospheric correction has been evaluated to be more efficient particularly in coastal areas, where the global atmospheric correction algorithm eventually fails to retrieve the water-leaving radiances (L_w) from satellite ocean color image data (Arnone et al., 1998). Atmospherically corrected L_w was subsequently converted to reflectance using $\rho = \pi L_w / F_o \cos\theta_o$ where F_o and θ_o are the mean extraterrestrial solar irradiance and the solar zenith angle respectively (Barnes & Zalewski, 2003). The atmospherically corrected reflectance, divided by π steradians, can be compared to the remote-sensing reflectance: $1/\pi\ \rho(\lambda) \approx R_{rs}(\lambda)$. The nL_w was calculated from $nL_w = F_o(\lambda)\, R_{rs}(\lambda)$.

3. Results and discussions

3.1. Description of observed radiance spectra and derivation of RI algorithms

This section describes variations of observed water-leaving radiance signals in response to the characteristics of water properties of the KSS, Korean southwest sea and YS (Fig. 2a–c). Note that appearance of *C. polykrikoides* bloom that discolored

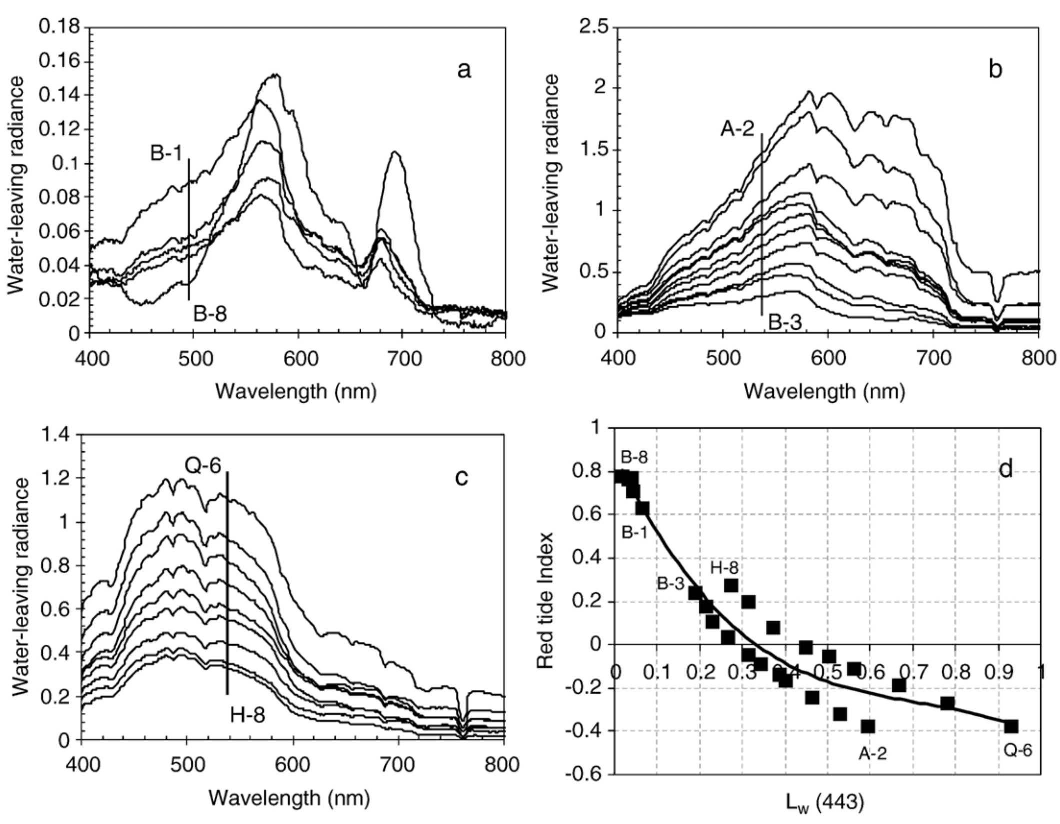

Fig. 2. (a–c) Variations in the water-leaving radiance (L_w) signals observed from the KSS red tide waters during August 2003 (a), Korean southwest sea turbid waters during September 2002 (b), and relatively clear southern YS waters during February 2003 (c). (d) Scatterplot of RI calculated using Eq. (5) versus L_w at 443 nm for $N=25$. Note that RI progressively increased with the decrease of L_w values at 443 nm (see the sample station number from B1 to B8 for red tide waters, A2–B3 for turbid waters and Q6–H8 for relatively clear waters).

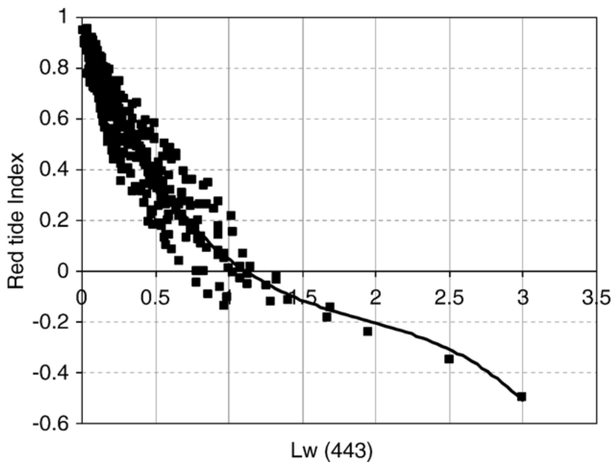

Fig. 3. Scatterplot of RI calculated using Eq. (5) versus L_w at 443 nm for data N=375, which were assimilated from a wide range of waters around Korean peninsula with Chl=0.1–107 mg m^{-3}, SSC=0.13–120 g m^{-3}, and DOM=0.01–2 m^{-1}.

waters of the KSS from blue to dark red/brown rapidly diminished the water-leaving radiance signal in the lower green and blue wavelengths part of the spectrum and increased the prominent signal in the green and red wavelengths part of the spectrum (Fig. 2a). This may be attributable to respective pigment backscattering between 550–565 nm and natural chlorophyll fluorescence around 685 nm, for Chl=6–70 mg m^{-3}; SSC=4–16 g m^{-3}; DOM 0.41–0.79 m^{-1} (Gitelson et al., 1994; Morel & Prieur, 1977). For estimating pigment concentrations in the oceanic waters, empirical algorithms take advantage of the decreased radiance or reflectance in the blue (440–490 nm) and the increased radiance or reflectance in the green region (550–565 nm), by working in terms of the ratios in these two wave bands (Gordon & Morel, 1983). The ratio at these two wavebands decreases as the chlorophyll concentration increases.

On the other hand, the water-leaving radiance spectra collected from highly turbid waters along the Korean southwest coastal areas increased with increasing SSC 4–95 g m^{-3} (Fig. 2b), where the concentrations of Chl and DOM ranged from 0.56 to 12.22 mg m^{-3} and 0.38 to 1.88 m^{-1}, respectively. High SSC occurred as a result of river discharge and the process of resuspension caused by strong tidal currents. Consequently, elevated SSC increased the backscattering more than the absorption towards longer wavelengths. This drew the attention of the researchers and encouraged them to exploit the usefulness of single band radiance or reflectance at these wavelengths for remote estimation of SSC from satellites (e.g., Ahn et al., 2001; Stumpf & Pennock, 1991). In cases of relatively clear and blue waters, the high L_w values occurred in the blue wavelength region and low L_w values in the longer wavelength region were observed. This suggests profound absorption by water itself, for conditions where Chl ranged from 0.43–1.32 mg m^{-3}, SSC from 3.33–10 g m^{-3} and DOM from 0.04–0.15 m^{-1} (Fig. 2c).

From the above data, red tide indices were calculated using Eq. (5) and then related to the absolute values of water-leaving radiance (L_w) at 443 nm to yield a new RI formula providing indices more responsive to variations of redness of the blooms and more resistant to some other environmental factors caused by lights and atmospheric conditions (Fig. 2d). Statistical analysis performed against these data revealed a goodness of fit represented by a cubic polynomial formulation with the correlation coefficient, R^2=0.94 and the number of observations, N=25 as follows,

$$\mathrm{RI}_{(\mathrm{DI})} = 10^{(-2.4394\times X^3+5.2587\times X^2-4.117\times X+0.8782)} \tag{6}$$

where $\mathrm{RI}_{(\mathrm{DI})}$ is the derived red tide index DI and X is the water-leaving radiance (L_w) at 443 nm. The performances of other formulations (e.g. linear, exponential, power) were also examined to illustrate their relative merits, but the findings suggested that cubic polynomial formulation (i.e., a third order polynomial) was superior to all other methods as reported in O'Reilly et al. (1998). A large number of data from different cruises covering a range of environments from typical red tide waters to turbid and clear waters off the Korean coast were pooled into this relationship which gave a new set of regression coefficients (Fig. 3) with slightly decreased correlation coefficient R^2=0.92 as follows,

$$\mathrm{RI}_{(\mathrm{DII})} = 10^{(-0.1069\times X^3+0.6259\times X^2-1.3936\times X+0.919)} \tag{7}$$

where $\mathrm{RI}_{(\mathrm{DII})}$ is the derived red tide index DII and X is the water-leaving radiance (L_w) at 443 nm. The total number of observations (N) was 375. A similar regression accomplished from nL_w values showed a notably decreased correlation coefficient R^2=0.88 for same number of in-situ observations (not shown).

3.2. Performance of RI methods and parameter selection

The behavior and effectiveness of RI methods were assessed by different parameters and spectral ratios using in-situ data and SeaWiFS ocean color image data (28 September 2003) representing a wide range of waters with intensive red tide blooms in the KSS and ECS. Table 2 shows that RI calculation based on the ratio 510/555 (adopted in Eq. (5)) tended to produce higher ranges of indices, regardless of parameters, followed by the blue green ratios 490/555 and 443/555. The resultant indices ranges were also dependent upon the parameters employed in Eq. (5): i.e., $[L_w(510)/L_w(555)-L_w(443)]/[L_w(510)/L_w(555)+L_w(443)]$, $[R_{rs}(510)/R_{rs}(555)-R_{rs}(443)]/[R_{rs}(510)/R_{rs}(555)+R_{rs}(443)]$, $[nL_w(510)/nL_w(555)-nL_w(443)]/[nL_w(510)/nL_w(555)+nL_w(443)]$, and $[R_{rs}(510)/R_{rs}(555)-nL_w(443)]/[R_{rs}(510)/R_{rs}(555)+nL_w(443)]$. It seemed

Table 2
Evaluation of the performances of RI methods based on different parameters and band ratios using in-situ optical data

Parameter	Ratio		
	510/555	490/555	443/555
R_{rs}	0.772–0.999	0.776–0.999	0.783–0.999
nL_w	−0.902–0.885	−0.912–0.886	−0.92–0.863
nL_w and R_{rs}	−0.914–0.919	−0.919–0.909	−0.92–0.901
L_w	−0.67–0.972	−0.675–0.965	−0.679–0.958

that the combined use of R_{rs} and nL_w was more appropriate for the RI calculation than the use of individual parameters nL_w and L_w. Here R_{rs} was not ideal because it did not yield a sufficient range of indices for characterizing red tide blooms from different water types. Notice the undervalued indices produced by nL_w and $R_{rs}+nL_w$ which are illustrated in Fig. 4a–c from SeaWiFS image of 28 September 2003. Comparisons between red tide indices of L_w and R_{rs}, nL_w, and $R_{rs}+nL_w$ indicate the lower range of indices associated with R_{rs} and undervalue indices with nL_w, and $R_{rs}+nL_w$. These may be attributable to the factors determining the shape and magnitude of nL_w spectra. To illustrate the merit of a three band RI fitted by cubic polynomial equations, the relationship between these indices was examined. A nearly linear fit was found for red tides and a downward curve fit was found for clear and turbid waters. This is consistent with an underestimation of indices given by Eq. (7) (Fig. 4d). However, a greater range of indices associated with a cubic polynomial function facilitates improved detection and delineation of HABs from other optical water types as described in the following sections.

3.3. Atmospheric correction by standard atmospheric correction (SAC) method and SSMM

The complex path signal (photons scattered due to air molecules, aerosols, and the air–sea interface) contributing approximately 80% to the total signal recorded at the top of the atmosphere (TOA), was effectively removed from the SeaWiFS data using SSMM. Examples of the desired water-leaving radiances from SeaWiFS images for 27 March 2002 and 28 September 2003 are presented in Fig. 5a–c and e. Overall, the shape and magnitude of L_w spectra retrieved from the SSMM were comparable with in-situ spectra, but an inappropriate

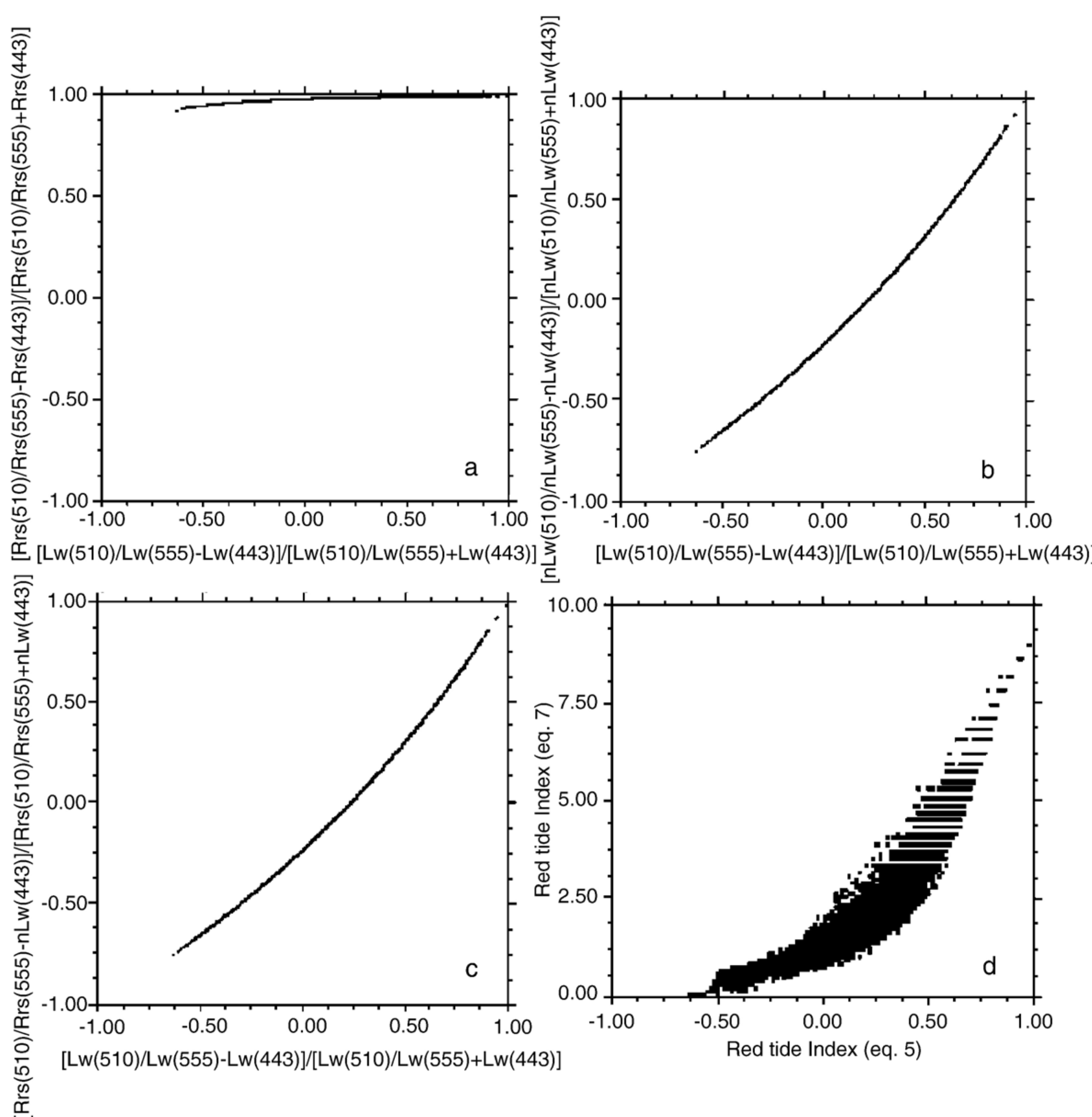

Fig. 4. (a–c) Comparison between the red tide indices estimated from SeaWiFS data on 28 September 2003 using following parameters L_w, nL_w, R_{rs}, and nL_w+R_{rs} adopted in Eq. (5). (d) Comparison between the red tide indices from Eqs. (5) and (7) (cubic polynomial).

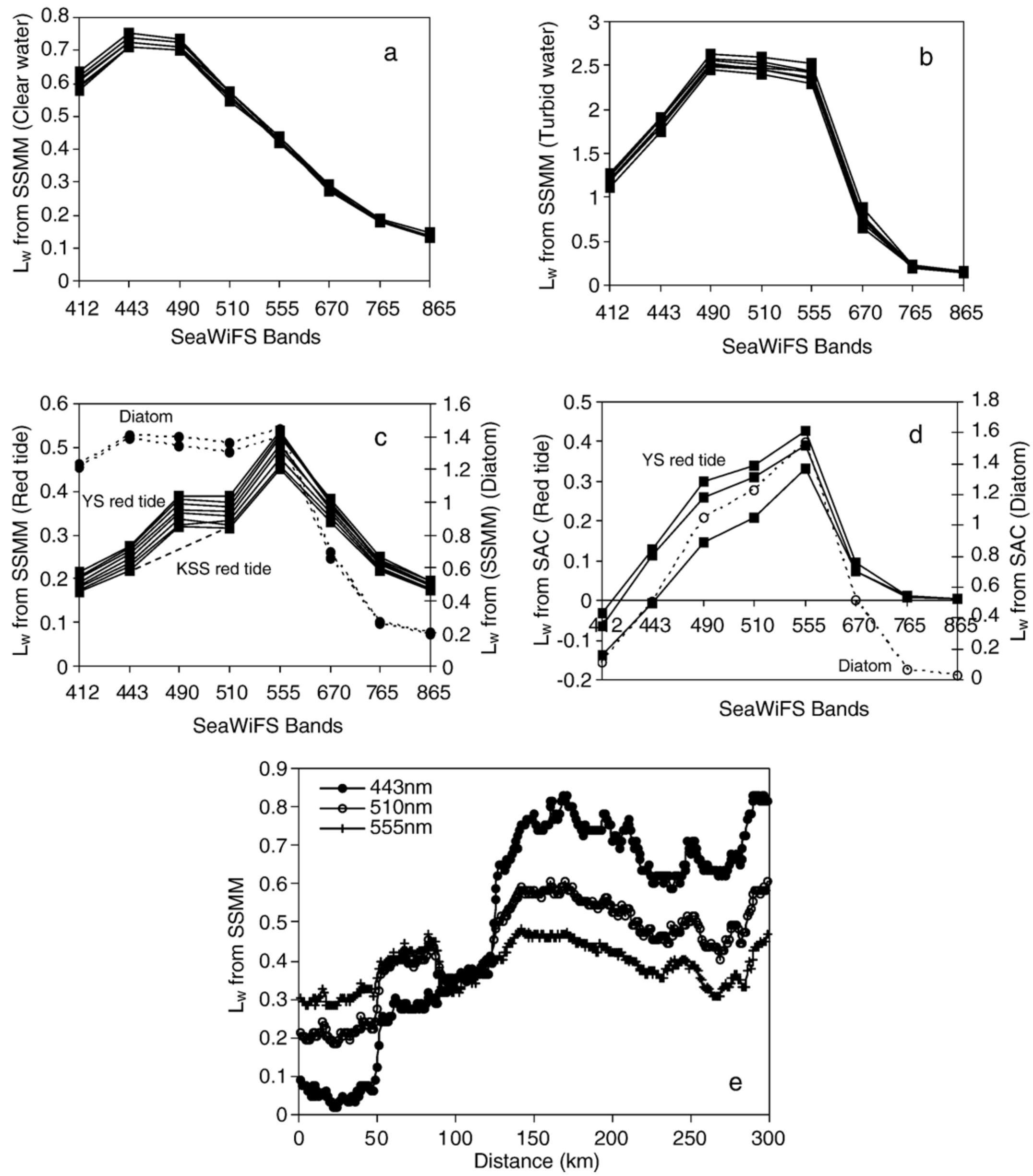

Fig. 5. (a–e) Spectral water-leaving radiances (L_w) (mW cm^{-2} μm^{-1} sr^{-1}) extracted from the SSMM atmospheric correction performed on SeaWiFS images of 27 March 2002 (a–d) and 28 September 2003 (e). The shape and magnitude of L_w spectra of clear, turbid, and red tide waters determined by SSMM appeared to be consistent with those of in-situ spectra. (c and d) Comparison of the results of SSMM and SAC algorithm in the YS red tide waters and diatom-dominated Korean west sea coastal waters. (e) East–west transect is running in the ECS/JS offshore from red tide areas to relatively clear waters (see the transect in Fig. 6c).

atmospheric correction performed using the standard SeaWiFS atmospheric correction (SAC) algorithm revealed an underestimation of L_w and frequently yielded negative L_w values in the red tide dominated YS waters during 27 March 2002 (Fig. 5d). These negative L_w values are due primarily to waters containing large accumulations of red tide species having a significant water-leaving radiance in the red and near-infrared bands, which could lead to possible errors in the atmospheric correction and underestimation of L_w in the blue and green bands of SeaWiFS. Arnone et al. (1998) who concentrate on coastal ocean optics/turbid water problems have first reported this, followed by the three studies of the same period (Hu et al., 2000; Ruddick et al., 2000; Siegel et al., 2000).

Successful atmospheric correction should enable accurate extraction of L_w in all bands representing significant spectral variations between the blooms of different phytoplankton species and the highly reflective waters of the region's Case-2 water environment. However, SAC algorithm appeared to distort the L_w spectra that seemed to be similar in shape for both diatom blooms along the west coastal areas and red tide dinoflagellate blooms in the YS offshore domain (Fig. 5d). This was in contrast with atmospheric correction done by SSMM that demonstrated large differences in the L_w spectral values for these same blooms, i.e., the YS red tide bloom would have higher magnitude of $L_w(555)$ and lower magnitude of $L_w(443)$, $L_w(490)$ and $L_w(510)$, whereas the diatom bloom increased the values of $L_w(412)$, $L_w(443)$, $L_w(490)$, $L_w(510)$ and $L_w(555)$ and thereby the spectral shape became nearly flattened in the blue and green region and steepened towards the red and near-infrared regions (Fig. 5c). The L_w spectra of the KSS red tide appeared to be similar to those of YS red tide, but with absence of a "shoulder" at $L_w(490)$ (dotted line in Fig. 5c) shown in Ahn et al. (2006). This may be attributed to differences in the composition of diatom and dinoflagellate species.

In KSS and ECS, a large difference in the values of L_w between the red tide bloom and adjacent clear oceanic waters was also apparent in an approximately 300 km (a SeaWiFS pixel is 1 × 1 km) east–west transect of $L_w(443)$, $L_w(510)$ and $L_w(555)$ extracted from the SeaWiFS image of 28 September 2003 using SSMM (Fig. 5e). The beginning of the transect shows intense patches of red tide bloom which can also be seen in the color composite SeaWiFS image (Fig. 6c). Notice that the regions of red tide bloom between 0–50 km exhibited very low $L_w(443)$ followed by $L_w(510)$ and $L_w(555)$. The observed difference between the values of $L_w(443)$, $L_w(510)$ and $L_w(555)$ slightly reduced in the waters containing lower concentrations of red tide algal matters from 50–130 km. However, in the transect from 130–300 km a reverse trend existed in the values of $L_w(443)$, $L_w(510)$ and $L_w(555)$ that varied uniformly, with $L_w(443)$ reaching highest, followed by $L_w(510)$ and $L_w(555)$, suggestive of clear oceanic waters of Kuroshio flowing from SW to NE.

3.4. Comparison between SeaWiFS chlorophyll and RI

Two chlorophyll algorithms, the OC4 and local Chl algorithm (hereafter referred as LCA, developed by Ahn & Shanmugam, in press), were employed to the SeaWiFS data collected on 28 Sep. 2003. The LCA algorithm is defined as follows

$$\langle \mathrm{Chl} \rangle (\mathrm{mgm}^{-3}) = 2.97X^{-4.49} \tag{8}$$

where X is the ratio $[R_{rs}(490)/R_{rs}(555)]$. The correlation coefficient (R^2) (for N = 118) is 0.85. The inferred Chl patterns from the OC4 and LCA algorithms were compared with the corresponding SeaWiFS color composite image and RI image from Eq. (7) (Fig. 6a–d). The findings revealed that the OC4 Chl increased from about 2 mg m^{-3} Chl offshore of the ECS to >15 mg m^{-3} Chl nearshore of the KSS (Fig. 6a). The elevated

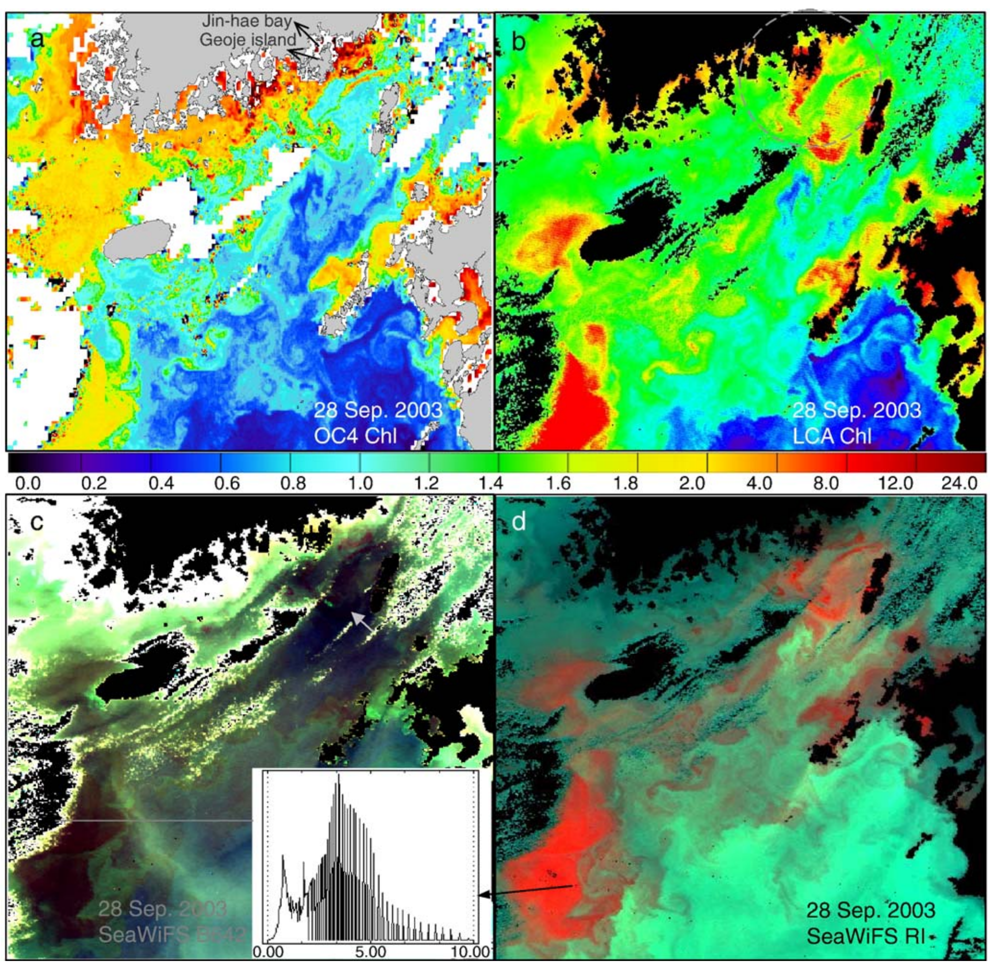

Fig. 6. (a) SeaWiFS Chl image processed using standard SAC algorithm and OC4 algorithm (Eq. (4)). (b) SeaWiFS Chl image resulted from SSMM and LCA algorithms. (c) Color composite image from water-leaving radiance (extracted from SSMM) in three SeaWiFS wavelengths: 670 nm (red), 510 nm (green) and 443 nm (blue). (d) Red tide index (RI) image processed using the cubic polynomial Eq. (7) is displayed with layers of the spectral ratios used in OC4 algorithm [i.e., RI (red), $L_w(510)/L_w(555)$ (blue) and $L_w(490)/L_w(555)$ (green)]. The distribution of RI values is displayed in the lower left corner of (d).

Chl levels observed off the Korean Southwest Sea (SWS) coastal areas are likely due to the presence of large amounts of non-pigment particulate and dissolved materials that appeared to potentially limit the utility of satellite-derived Chl for this application (Ahn et al., 2006; Cannizzaro et al., 2002; Tang et al., 2003). For areas where moderate SSC and intense HABs were encountered offshore, the OC4 algorithm exhibited nearly homogeneous Chl patterns that were inconsistent with those seen in the LCA Chl image (Fig. 6b). The discrepancy between these two images may have resulted from the failure of SAC algorithm and/or OC4 algorithm. However, the LCA Chl image was achieved by applying the SSMM atmospheric correction and LCA developed using our bio-optical data (N=132 representing waters with Chl 0.1–115 mg m^{-3}, SSC 0.15–120 g m^{-3} and DOM 0.01–2 m^{-1}). When the SSMM atmospheric correction was able to recover areas of highly reflective waters that were previously masked by the SAC algorithm, the LCA performed noticeably better minimizing errors in most areas (with the exception of Korean southwest coastal waters). Stumpf (2001) has cautioned against using such an algorithm in these exceptional areas. Overall, LCA Chl estimates differed from those of OC4, yielding high Chl for red tides and low Chl for non-bloom and turbid waters around KSS and ECS (Fig. 6b). The spatial variability of red tide intensity offshore characterized by the LCA showed good agreement with those patterns inferred from the color composite image and RI image (Fig. 6c and d).

The color composite (B642) SeaWiFS image, processed by manipulation of the range of digital radiance values graphically represented by its histogram, consisted of considerable spatial variability characterized by three different color ranges corresponding to different levels of red tide accumulation (Fig. 6c). In this figure, the dark violet features show evidence of the presence of HABs in the nearshore and offshore waters characterized by much weaker radiances in the red and blue wavelength bands, while the brighter features relate to highly reflective materials (such as sediments) along the Korean southwest sea coastal areas caused by strong radiance in the green wavelength band. However, in some areas off the Korean southern coast (indicated by an arrow) the strong patchiness of HABs was not obvious. These areas might have produced significantly weaker radiances in these bands, due to mixing of offshore water mass by the action of a local eddy feature inferred from AVHRR sea surface temperature (SST) image (not shown).

In contrast, the RI algorithm (Eq. (7)) provided a synoptic range of indices capturing the spatial variability of red tide blooms that began in the nutrient-rich ECS waters and coastal waters of KSS (Fig. 6d). The red tide indices varied from 0–0.5 for extremely turbid waters with very high SSC and DOM, 0.5–1 for relatively clear waters with less algal matters, 1–3 for waters with less intense HABs and >3 for dense waters with HABs. Higher indices of red tide waters off the Geoje island to the east of KSS were related to *C. polykrikoides* cell abundance 1×10^3–22×10^3 cells ml^{-1} which was observed by National Fisheries Research and Development Institute (NFRDI) in the Korean South Sea Coastal Areas (SSCA) and Korean East Sea Coastal Areas (ESCA) (Fig. 7). The indices of <3 represented *C. polykrikoides* cell concentrations $<2\times10^3$ cells ml^{-1} in the ESCA.

3.5. Relationship between RI and Chl

The relationship between the Chl and RI was examined with the aim to quantify the concentrations of HABs from other properties of waters in the Korean and neighboring seas. Fig. 8a and b compare the SeaWiFS RI (calculated from Eqs. (5) and (7)) and LCA Chl concentrations covering a wide range of waters with a massive red tide bloom episode on 28 September 2003. Notice that RI estimates using Eq. (5) exhibited an inverted heart-shaped scatters that did not represent a good correlation with varying LCA Chl concentrations 0.2–16 mg m^{-3} (Fig. 8a), whereas RI estimates from the cubic polynomial formulation (Eq. (7)) appeared to have good consistency with LCA Chl concentrations and clearly illustrated the possibility of achieving accurate estimates of Chl over red tide dominated waters (Fig. 8b). Bio-optical data collected from typical red tide waters of KSS, turbid waters of SWS and relatively clear waters of YS and ES during 2002 and 2003 cruises were analyzed to evaluate the consistency of RI–Chl relationship. Fig. 8c makes obvious that the RI estimates from Eq. (7) ($RI_{(DII)}$) are most consistent with log-transformed in-situ Chl concentrations 0.6–82 mg m^{-3}. The inset shows how the untransformed data of Chl and RI were scattered — the results closely matching with those illustrated in Fig. 8b. Statistical regression analysis of RI performed against the in-situ Chl data (N=41) yielded a Red tide index Chlorophyll Algorithm (RCA) as follows,

$$\langle Chl\rangle(mgm^{-3}) = 0.316e^{(0.61\times RI_{(DII)})} \quad (9)$$

with the correlation coefficient R^2=0.92. This equation reveals that in-situ Chl concentrations correspond best with an exponential rather than a linear function of RI and the high value R^2 illustrates a strong performance of such an index for

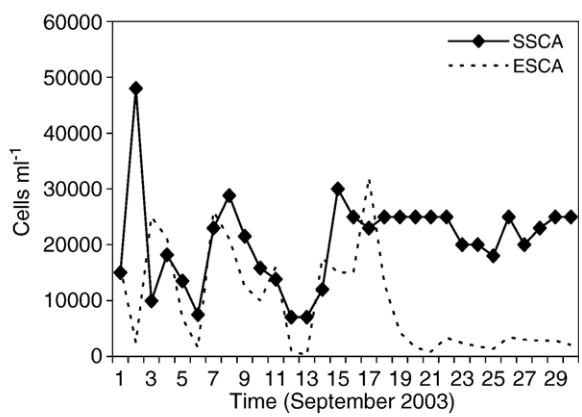

Fig. 7. Field data of *C. polykrikoides* cell abundance observed by NFRDI in the Korean SSCA and ESCA during September 2003. Note that elevated cell concentrations occurred all the time through September in the SSCA, but in the Korean ESCA the cell abundance rapidly decreased following the period of weakened EKWC along the Korean east coast after 20 September 2003. The detached patterns of red tides from ESCA indicated this to be shown in Fig. 6d.

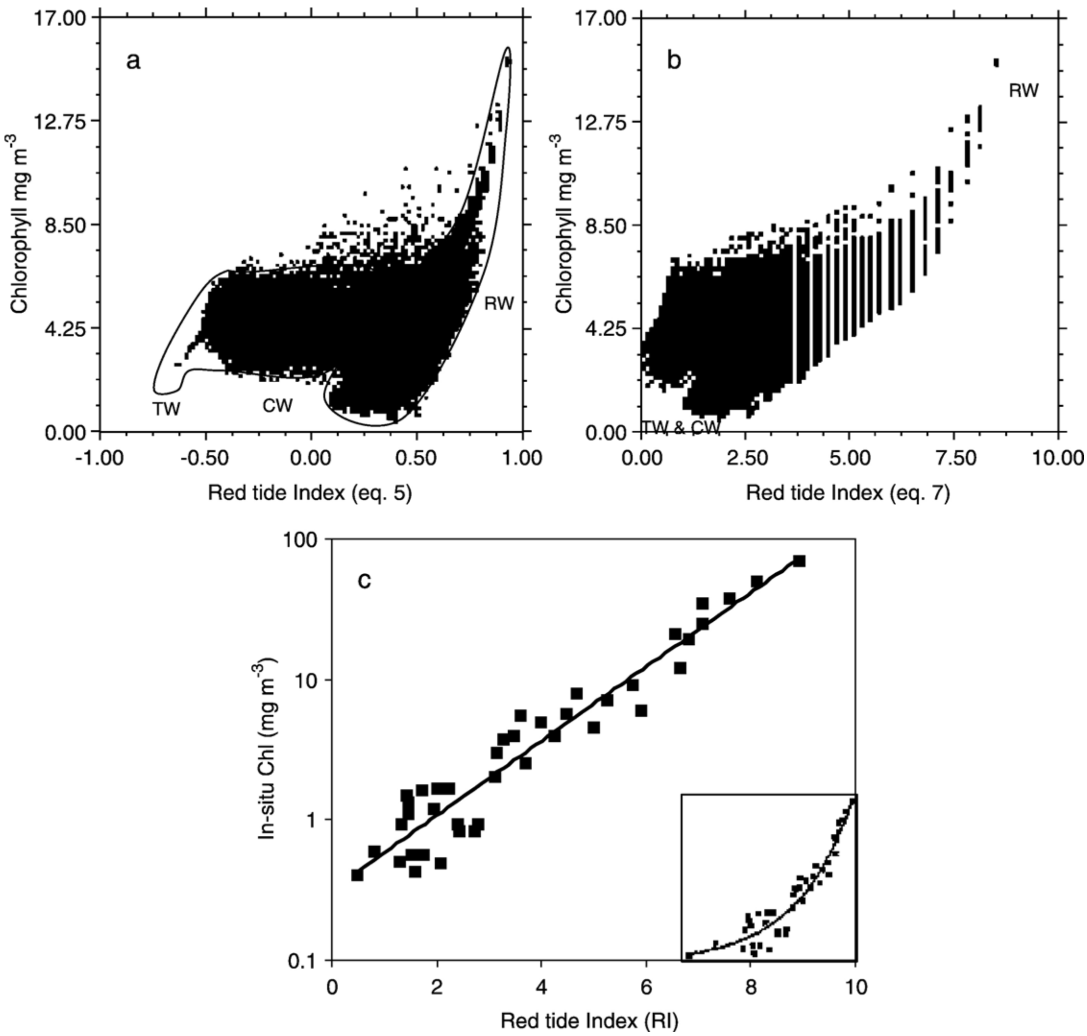

Fig. 8. (a and b) Comparison between the RI calculated using Eqs. (5) and (7) and Chl concentrations. (c) RI from Eq. (7) versus log-transformed Chl data (N=41) collected from in-situ measurements over the KSS red tide waters, SWS turbid waters and relatively clear ES and YS waters during 2000, 2002 and 2003 cruises. The inset shows untransformed data of RI and Chl matching closely with that seen in (b) TW — turbid water, CW — clear waters, RW — red tide waters. Note that the above relationships do not represent waters of other phytoplankton blooms (non-HABs).

estimating Chl for waters containing HABs. The derived Chl values are red tide specific and therefore can be used to quantitatively detect and assess the potential areas of HABs in optically complex waters.

3.6. Applications to regional waters

The established algorithms were applied to SeaWiFS images of spring from 1999–2002 and the results were compared with those of OC4 algorithm in the ECS, BS and YS (Figs. 9a–d, 10a–d and 11a–d). OC4 Chl concentrations appeared to be drastically increased in most of the coastal areas, including aerosol-dominated areas to the western part of Korean peninsula during March 2002. This suggests the potential response of OC4 algorithm to materials other than phytoplankton in these areas. In contrast, the RI images displayed with layers of the spectral ratio used in OC4 algorithm [i.e., RI (red), $L_w(490)/L_w(555)$ (green), and $L_w(510)/L_w(555)$ (blue)] provided an enhanced understanding of the spatial and temporal variability of different phytoplankton blooms that initiated under favorable light and nutrient conditions of the spring. Consider the ECS; the April 1999 image is a good example of how the overstated OC4 Chl is coupled with water masses characterized by cross-shelf transport of Yangtze River materials to the Korean sea for which the RI values were typically below 0.5 (in green color) (Figs. 9a and 10a). But for areas denoted by a solid line box in Fig. 10a, noticeable patches of phytoplankton bloom detected by OC4 Chl around the western inner shelf areas of ECS were spatially consistent with those inferred from the RI image (0.7–1.1). These patches, coinciding with relative low temperature, homogeneous vertical profiles and low water column depth (<25 m), may be attributable to a dominant spring diatom bloom contributing at least 80% of the total phytoplankton mass in these areas (Furuya et al., 1996; Hong, 2003). Application of RCA yielded Chl values <0.6 mg m^{-3} supporting their previous hypothesis of observing no identifiable HABs occurring in these areas during spring (Fig. 11a). However, the diatom blooms disappear soon after a rapid exhaustion of essential

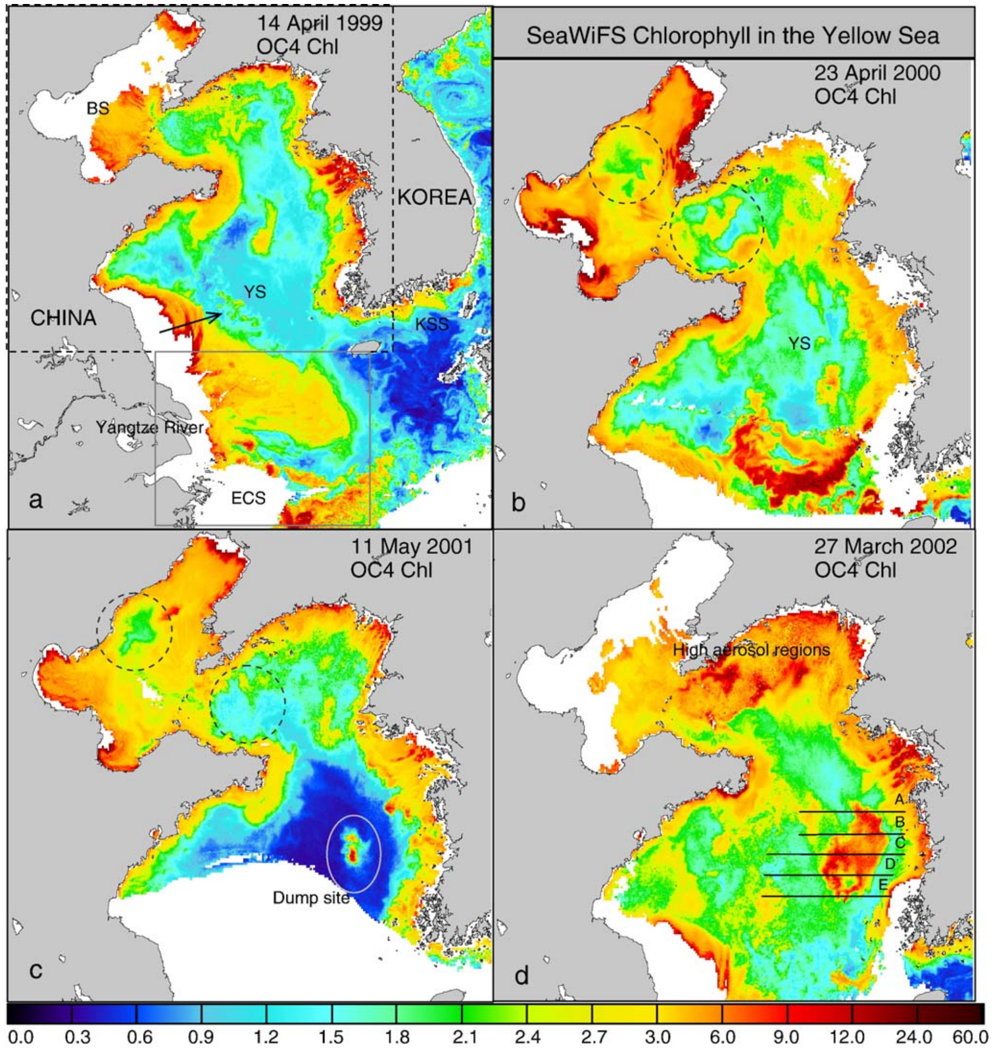

Fig. 9. (a–d) The OC4 Chl for the period of spring from 1999–2002 in the ECS, YS and BS. The SAC algorithm was used to correct the atmospheric effects in the SeaWiFS images, creating mask over coastal areas. The cruise transects are illustrated for 27 March 2002 (d).

nutrients in May and HABs eventually reemerge at surface waters replenished with nutrients from the Yangtze River during the longer day lengths of summer and fall seasons. These HABs grew species quicker with an average abundance of 7.3×10^5 cellsl^{-1} (Gao & Song, 2005).

In the BS region, the OC4 algorithm produced abnormally high Chl concentrations (>15 mg m^{-3}) in proximity to the coast which is subjected to huge amounts of SSC and DOM discharged from the 17 rivers nearby. The OC4 algorithm also gave a negative indication for the presence of a HAB in the circled areas to the north and southeast (entrance) of BS (Fig. 9b and c). The lack of a HAB signature depicted from the OC4 algorithm may be caused by ineffective atmospheric corrections by the SAC algorithm and/or the standard spectral ratios bio-optical algorithm. Once again the RI and RCA algorithms provided a more comprehensive assessment about the existence of different algal blooms and their controlling optical properties (Figs. 10a–d and 11a–d). In RI images three kinds of signatures can be discerned: (1) green color with very low indices <0.5 (extremely turbid), (2) brown color with low indices between 0.7–1.1, and (3) red color with high indices >2. The moderate RI (brown color) supports previous investigations of spring diatom blooms in the western and southern parts of the BS (Fig. 10a), where the diatom cells were reported to be small in size reaching a maximum in April and a minimum in September 1999 (Wei et al., 2004). Chl concentrations over diatom-dominated waters ranged between 0.16–7 mg m^{-3} with a mean concentration of 1.62 mg m^{-3}. Ship survey data of the above authors suggests that diatom populations thrive under favorable nutrient and light conditions at the surface where the water is slightly warm (5–11 °C) and weakly stratified during this period.

Figs. 10b and 11b display a clear picture of the development and southward drifting of a massive HAB episode on 23 April 2000 in the BS. For intense HAB areas (in the northern part and entrance of the BS) RI was >2.5 corresponding to a RCA Chl estimate of 3–10 mg m^{-3}. Less dense and discrete patches of HAB were also observed with slightly decreased RI 1.1–2.5 corresponding to a RCA Chl estimate of 0.8–3.3 mg m^{-3}. The discrete patches were intermingled with diatom blooms yielding RI<1.1 to the southwest BS. Changes in water temperature

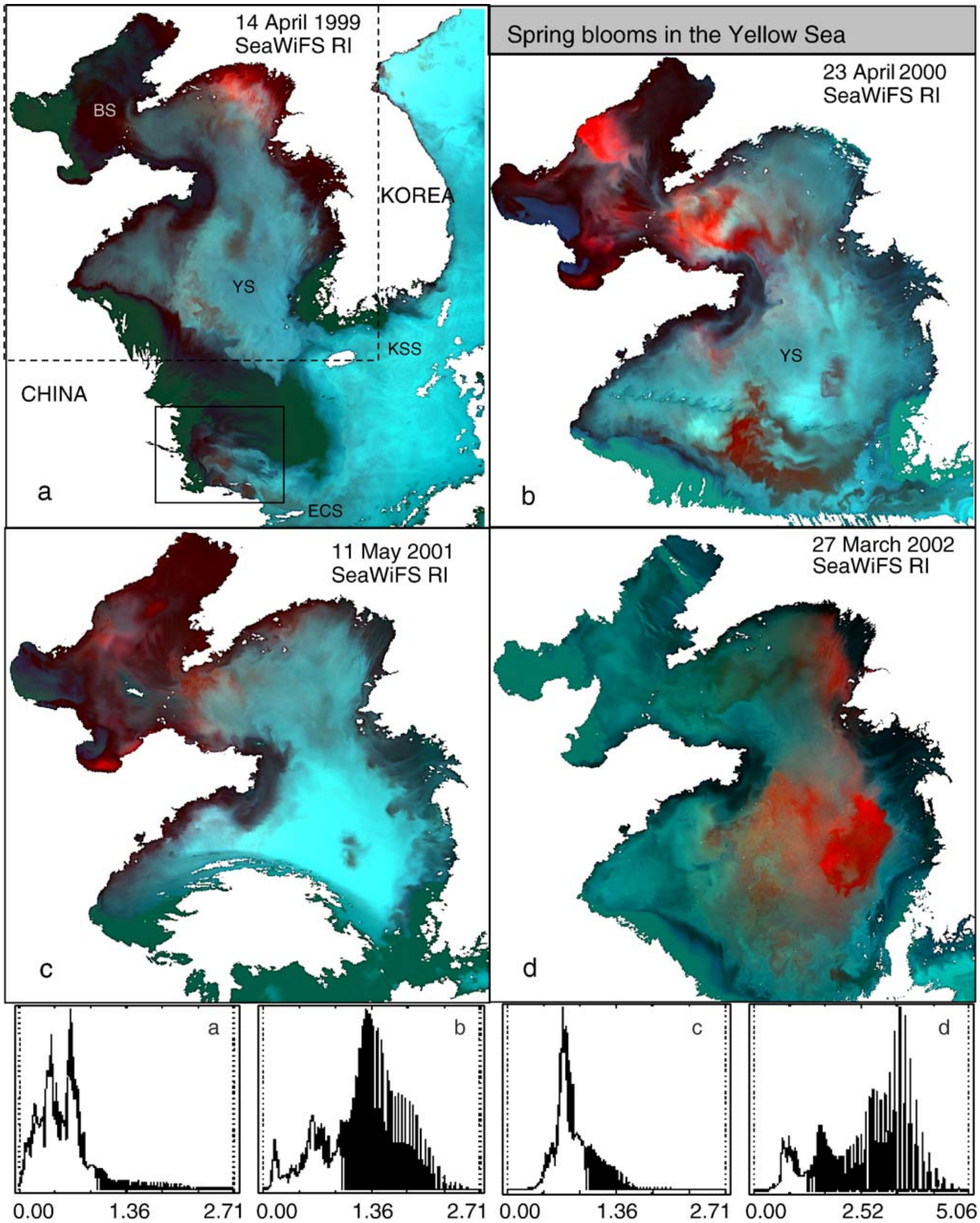

Fig. 10. (a–d) SeaWiFS RI images (using Eq. (7)) displayed with layers of the spectral ratios used in OC4 algorithm [i.e., RI (red), $L_w(490)/L_w(555)$ (green), and $L_w(510)/L_w(555)$ (blue)] exhibit various types of algal blooms in the ECS, BS and YS. Atmospheric correction was performed with SSMM. Red color — HABs, brown color — non-HABs (diatom blooms), green color — highly turbid waters, dark blue — water containing high suspended sediments and dissolved materials, cyan color — relatively clear waters. The corresponding indices values (x axis — RI; y axis — frequency) are displayed in the bottom panels.

combined with weak stratification of anthropogenically dominated coastal waters have been reported to cause frequent occurrence of HABs imposing serious economic losses totaling over 62 million US$ in 1998 (EQB, 2000). These anthropogenically derived HABs appear to move southward from the northern BS and expand to form a tongue-shaped patch towards the southern YS where the ocean is characterized by a vertically mixed layer of waters of warmer temperature and salinity due to the intrusion of the YSWC (Fig. 11b). Previous studies could not detect offshore drifting of HABs in the southern BS and YS because of inconclusive evidence derived from standard Chl algorithms (Tang et al., 2006) or because of limitations in field measurements at discrete points during ship surveys (Wei et al., 2004). For example, RCA Chl in the southern YS was found to be <2 mg m^{-3} in contrast with OC4 Chl showing >10 mg m^{-3}. The intense phase of a HAB around the entrance of the BS, may be related to the hypothesis that strong northwest winds transport surface waters southward, causing previously accumulated nutrient regime waters below the euphotic zone to be displaced northward. Such large scale circulation driven by strong winds could lead to a vertically mixed homogeneous water mass allowing nutrients to become enriched in the euphotic zone stimulating rapid growth of HABs and, ultimately, causing a collapse of the ecosystem at the entrance of BS (Goa, 1994).

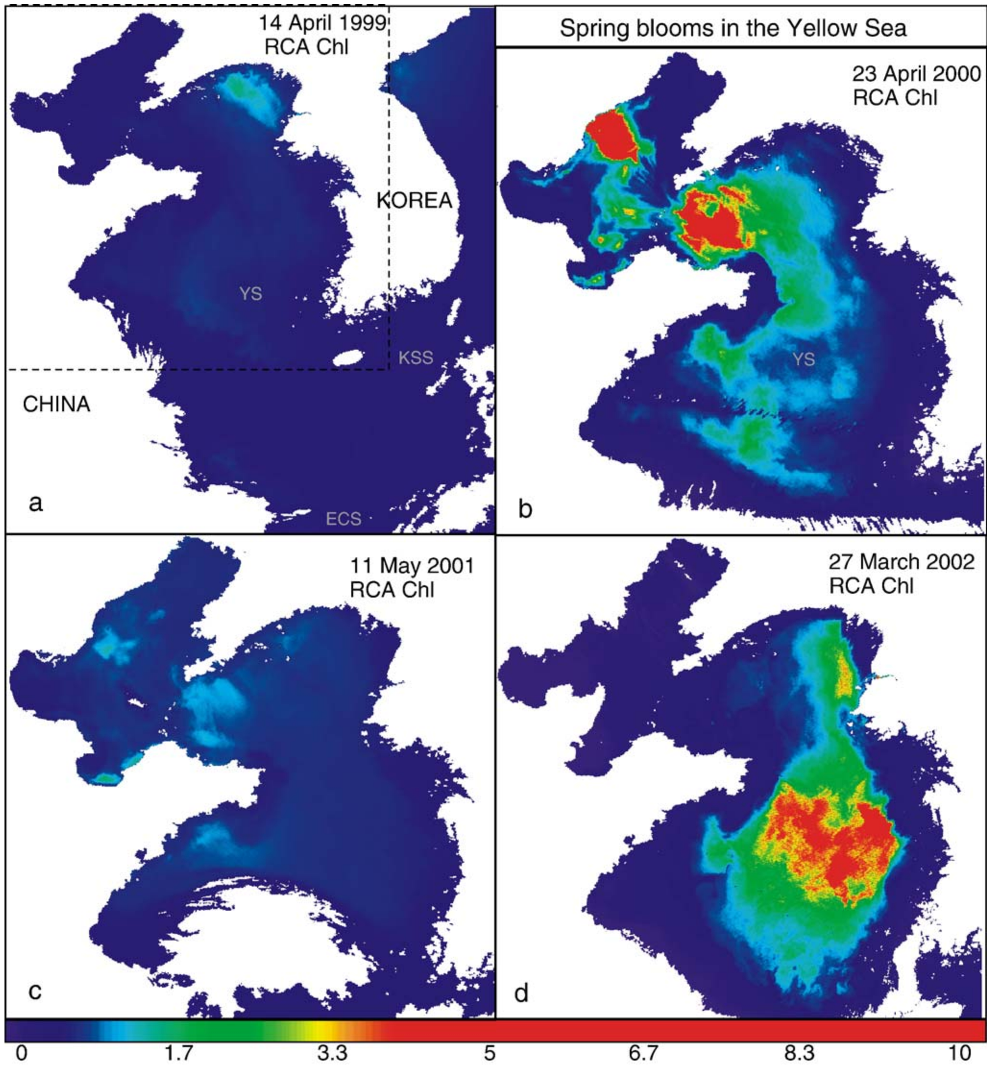

Fig. 11. (a–d) RCA Chl for the period of spring from 1999–2002 in the ECS, YS and BS. SSMM was employed for correcting atmospheric effects in the SeaWiFS images.

The applicability of OC4, RI and RCA algorithms were also assessed for predicting red tide blooms of the YS. Here we gave importance to the well outlined patches observed on 11 May 2001 and 27 March 2002 images (Figs. 9c and d, 10c and d and 11c and d). The OC4 algorithm appeared to indicate the presence of phytoplankton bloom (Chl 1.5 to 7 mg m^{-3}) around a "dump site" in the central part of YS (Fig. 9c), where RI gave indices of <0.6 implying this water mass had high turbidity as a result of nonpigment dumped materials (Fig. 10c) (Ahn et al., 2004). The RCA Chl showed no signs of a HAB around this area during May 2001, consistent with the nutrient-depleted stratified waters of the summer period (Lie et al., 1999). On 27 March 2002, there was a sign of HABs in the YS (Figs. 9d, 10d and 11d). OC4 gave a good indication of this bloom but with less detail on its spatial characteristics. In contrast, RI and RCA Chl captured apparent patterns of red tides and suggested that highly concentrated red tide patches were associated with the eastern boundary with less dense and spatially diffused patterns extending as far as the western boundary and southern YS.

To better illustrate the difference between the established algorithms, NFRDI cruise data consisting of Chl, nutrients (SiO_2^-S, NO_3^-N, $PO_4^-P^-$), temperature (°C), and salinity (psu) collected prior to the initiation and during the decomposition phase of an encountered HAB in the YS during mid-February and the first–second week of April 2002 respectively were used (Fig. 12a–c) (see cruise transect in Fig. 9d). Five transects, A, B, C, D and E, were established traversing across the bloom from bright (high relative reflectance) cold coastal waters in the east to dark (relatively weak reflectance) warm and saline offshore waters in the west. In-situ Chl concentrations from each transect were compared with satellite-retrieved Chl using OC4, LCA and RCA (Fig. 12a). Note that because of time difference (as mentioned above) between satellite and field observations, the estimates of Chl by OC4, LCA and RCA differed from in-situ Chl data at several locations, particularly the nearshore stations A3, B1, C1, D3 and E5. The in-situ Chl showed a negative trend with satellite retrievals in these areas probably because of a high abundance of diatom populations along the coastal areas during

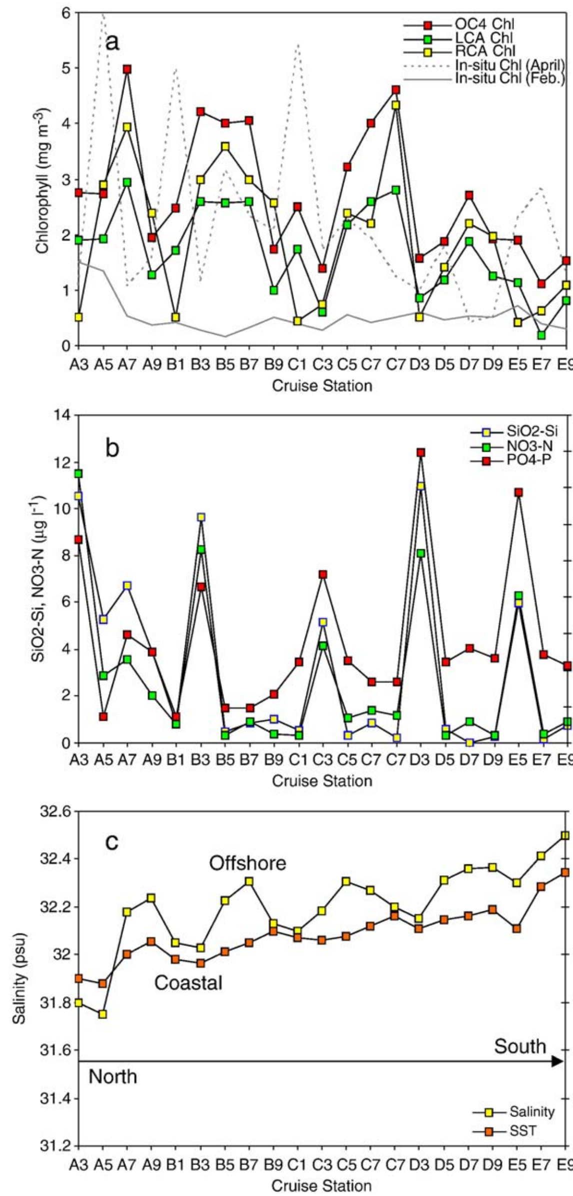

Fig. 12. (a) Comparison between the satellite and in-situ Chl concentrations (mg m^{-3}) at different cruise locations in the YS. (b and c) Horizontal profiles of SiO_2^-S, NO_3^-N, PO_4^-P, SST and salinity. In-situ observations took place before and during the decomposition phase of HAB in mid February and early-mid April 2002 respectively. The elevated Chl associated with waters of low nutrients and high temperature and salinity offshore are due to occurrence of HAB.

the first–second week of April 2002. However, the RCA Chl exhibited a good consistency with in-situ Chl for the offshore stations B5, C5 and D5 (red tides). Comparisons between the satellite Chl estimates showed that all three algorithms gave higher Chl estimates in nutrient-depleted warm and high saline waters offshore and lower estimates in nutrient-enriched coastal cold waters. However, a significant difference between these algorithms was noticed, i.e., the OC4 had the higher Chl values, RCA the moderate values and LCA the low values at all stations. At nearshore stations A3, B1, C1, D3 and E5, OC4 and LCA produced slightly elevated Chl, likely due to interference of high DOM concentrations and/or possibly high diatom concentrations along the Korean west coastal areas. RCA Chl estimate was <0.7 mg m^{-3} indicative of no HABs in these areas.

Nutrient and hydrography data (illustrated in Fig. 12b and c) revealed that surface water SiO_2^-S, NO_3^-N, PO_4^-P concentrations were associated with areas of low temperature and low salinity coastal current waters along the Korean west coastal areas (Sts. A3, B1, C1, D3 and E5). Despite high nutrient supply resulting from vertical mixing of the winter-accumulated nutrient regime below the euphotic layer, low nutrient concentrations were still observed in the surface waters of the central YS and could be due to the blooming of red tides. This bloom spanned more than one month due to weak veridical density gradient resulting from the increased irradiance occurring at this time, which ultimately increased the retention time of red tide phytoplankton in the surface mixed layer. The combination of enhanced irradiance with the effect of mixing of the YSWC and high-nutrient Yellow Sea Cold Water (YSCW) seemed to cause the spring bloom in the central YS (Hyun & Kim, 2003).

Fig. 13a–d compare the ability of detecting a highly toxic *C. polikrikoides* blooms by OC4 and RI algorithms applied to SeaWiFS image of 19 September 2000 in the KSS. This was a period of intensive HAB outbreaks and a large exchange between coastal and offshore water mass properties caused by coastal runoff and the intrusion of the TWC from offshore (Ahn et al., 2006). First note that areas with dense *C. polikrikoides* blooms around the semi-enclosed coastal bays masked by the SAC algorithm were successfully recovered by the SSMM method. In these areas, the bloom of *C. polikrikoides* gave higher indices (RI > 7 represented by red color in Fig. 13b) than those of other harmful algae observed in the BS and YS that exhibited RI < 4. RCA yielded Chl > 15 mg m^{-3} (Fig. 13c). The spatial patterns of high RI and RCA Chl were consistent with the intense phase of *C. polikrikoides* bloom ($>1.5\times10^4$ cells ml^{-1}), which drifted southwestward along the Kosong coastal areas of the KSS (Fig. 13b–d). In contrast, OC4 Chl revealed false information for many of these coastal areas potentially limiting the utility of SeaWiFS data for mapping and monitoring these red tide blooms in the KSS (Fig. 13a). Fig. 13e shows another example of RCA Chl demonstrating the detailed spatial variability of HAB occurrence on 28 September 2003 in the ECS and KSS.

4. Conclusions

Coastal eutrophication and enhanced nutrients concentrations offshore due to vertical mixing have been linked with the development of large biomass, ultimately leading to anoxia, toxic or harmful impacts (e.g., mechanical damage such as choking gills) on fisheries resources, ecosystems, and human health or recreation (Anderson et al., 2002; Burkholder, 1998; Shumway, 1990). One way to mitigate the potential impact of these blooms is to improve their detection by satellite. Several previous studies have approached this problem by using optical properties, spectral ratio discrimination, satellite chlorophyll anomaly, FLH algorithm, and climatological data analysis (Carder & Steward, 1985; Cannizzaro et al., 2002; Hu et al., 2005; Sarangi et al., 2004; Stumpf et al., 2003; Suh et al., 2004; Tomlinson et al., 2004; Zabicki, 1995). Some of these techniques have provided reliable

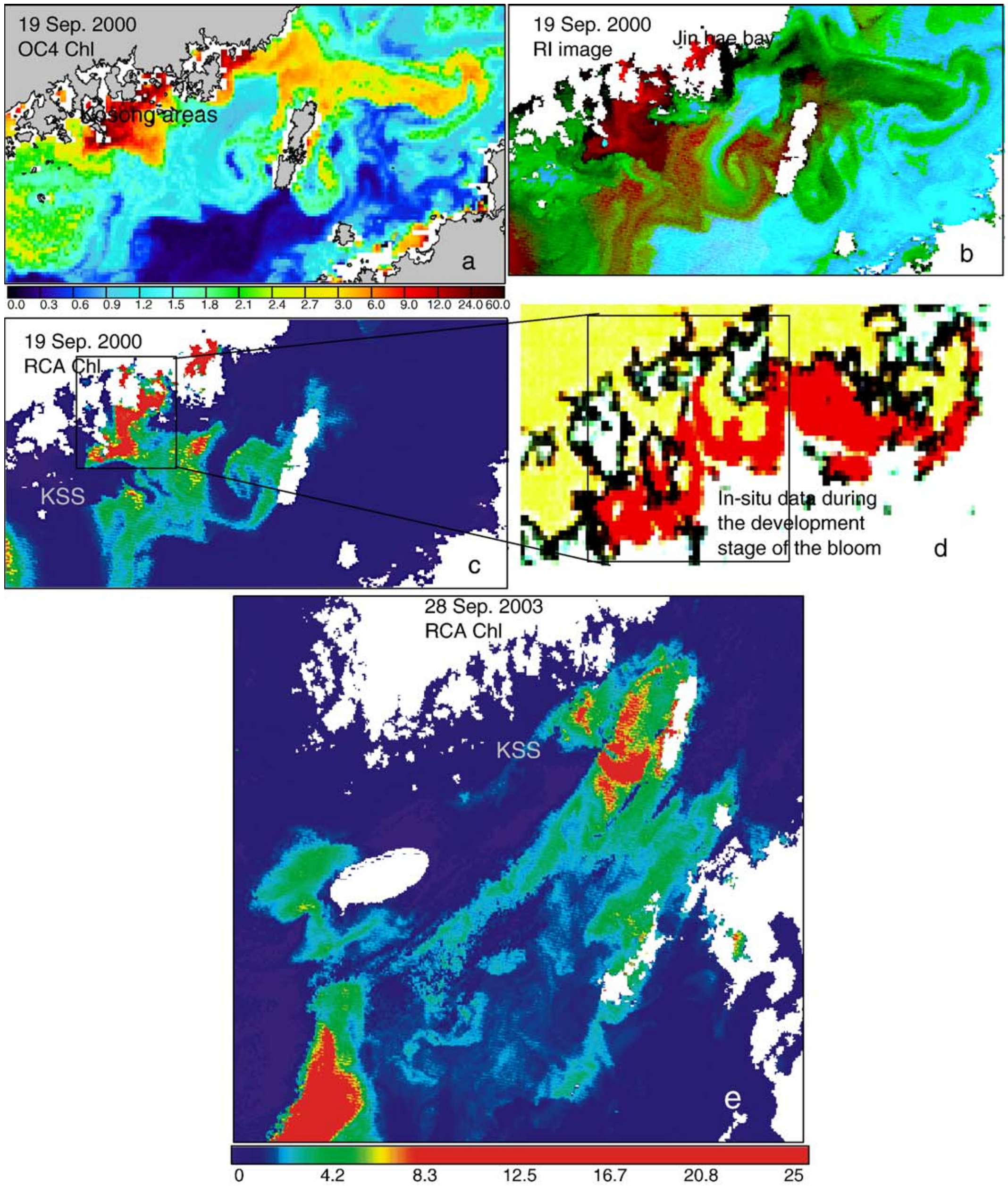

Fig. 13. (a–d) Comparison of red tide detection by SAC-OC4 and SSMM-RI algorithms applied to SeaWiFS image of 19 September 2000 in the KSS. (a) OC4 Chl image, (b) RI image, (c) RCA Chl image and (d) in-situ data collected from the KSS coastal areas during the early stage of *C. polykrikoides* bloom by NFRDI (Suh et al., 2004). Notice the RCA Chl showing good comparison with in-situ data limited to coastal areas, whereas the OC4 Chl does not. (e) The RCA Chl concentrations demonstrating the spatial variability of a massive HAB occurred on 28 September 2003 in the ECS and KSS. The RCA color scale is same for (c) and (e).

detection, but many cases were not able to fully support accurate identification, monitoring and forecasting of future locations of the HABs, particularly in optically complex Case-2 water environments. One of the main sources of inaccuracy is due to interference of high scattering and absorbing materials present in the water column. Inaccurate information derived from these methods prevents managers from better anticipating red tides or allowing them to better focus their sampling efforts on threatened aquaculture fish-harvesting areas, particularly in coastal oceanic ecosystems.

In describing remote detection of HABs we must address the potential sources of error that result from both the atmospheric correction algorithm and the bio-optical algorithm, commonly used to estimate Chl concentration in ocean waters (Gordon et al., 1980). First, one must account for the spectrally distorted and negative water-leaving radiances resulting from an inappropriate atmospheric correction by the SAC algorithm. Overcorrection of atmospheric effects has been observed to be severe in the blue spectral region and becomes progressively worse for productive waters with higher Chl concentration (>2 mg m^{-3}) (Arnone et al., 1998; Siegel et al., 2000). Second, the use of standard bio-optical algorithms that have been specifically developed for oceanic waters remains problematic in optically complex waters, because the simple blue and green band ratio used in regression analysis is not only sensitive to phytoplankton but also to other associated water constituents such as DOM and SSC (and perhaps even bottom effects), which lead to large errors in the satellite Chl retrieval for coastal waters (Darecki & Stramski, 2004; Montes-Hugo et al., 2005). Third, the combination of these errors limits the potential utility of satellite ocean color data for mapping likely areas of HABs and thus, ultimately, preventing the associated economic loss (Cannizzaro et al., 2002; Subramaniam et al., 2002).

Our approach to the red tide detection problem is based on an indigenous atmospheric correction method (SSMM) and RI algorithms developed by using in-situ bio-optical data collected from Korean seas and neighboring waters. Extraction of water-leaving radiances in all SeaWiFS bands was successful and spectral shape remained unaltered by the application of SSMM in optically complex waters (Ahn & Shanmugam, 2004; Ahn et al., 2006). The results of our investigation clearly show the advantages of applying RI and RCA algorithms over traditional spectral ratios methods to correctly identify the potential areas of HABs and distinguish other phytoplankton blooms from SSC dominated and non-bloom oceanic waters. The spatial patterns of red tides inferred from RI and RCA algorithms appeared to be more consistent with in-situ data than those from standard OC4 and LCA algorithms. We plan to extend our algorithms for detecting HABs to other regions and continue to future refine and validate previously established methods.

Acknowledgements

This is the post doctoral research work of Dr. P. Shanmugam on Development of Case-2 water bio-optical and atmospheric correction algorithms receiving support from the Ministry of Maritime Affairs and Fisheries (MOMAF) and Ministry of Science and Technology (MOST) (KORDI contract PM 294-00 and PN 524-00) through Prof. Yu-Hwan Ahn at Ocean Satellite Research Group. We thank Dr. Noh Jae-Hoon, KORDI and Dr. Lee-Hyun Jang, NFRDI for making available the CTD data, nutrients and chlorophyll data for this study. The authors would like to express their sincere gratitude to the Editor-in-Chief of the Remote Sensing of Environment, and Dr. Robert Arnone, Naval Research Laboratory (NRL), Stennis Space Center, MS, USA and the two anonymous reviewers for their valuable comments and suggestions, which helped improving the manuscript.

References

Ahn, Y. H., & Moon, J. E. (1999). Specific absorption coefficients for the chlorophyll and suspended sediment in the Yellow and Mediterranean Sea. *Journal of the Korean Society of Remote Sensing*, *14*, 353−365.

Ahn, Y. H., Moon, J. E., & Gallegos, S. (2001). Development of suspended particulate matter algorithms for ocean color remote sensing. *Korean Journal of Remote Sensing*, *17*, 285−295.

Ahn, Y. H., & Shanmugam, P. (2004). New methods for correcting the atmospheric effects in Landsat imagery over turbid (Case-2) waters. *Korean Journal of Remote Sensing*, *20*, 289−305.

Ahn, Y. H., & Shanmugam, P. (in press). Analysis of sun-induced fluorescence signal in relation to remote estimation of chlorophyll-a concentrations from the oceanic waters: Algorithm development and validation using in-situ bio-optical data. *International Journal of Geoinformatics*.

Ahn, Y. H., Shanmugam, P., & Moon, J. E. (2004). Spatial and temporal patterns in satellite-derived chlorophyll-a concentration and their relation to oceanic processes in the East China Sea and Yellow Sea. *Proceedings of the Spring Meeting of the Korean Society of Oceanography,* Pusan, Korea, 13–14 May, (pp. 183−190).

Ahn, Y. H., Shanmugam, P., Ryu, J. H., & Jeong, J. C. (2006). Satellite detection of harmful algal bloom occurrences in Korean waters. *Harmful Algae News*, 213−131.

Anderson, D. M. (1998). *Study of red tide monitoring and management in Hong Kong: literature review and background information. Technical Report*, *Vol. 1*. Hong Kong: Hong Kong Agricultural and Fisheries Department.

Anderson, D. M., Glibert, P. M., & Burkholder, J. M. (2002). Harmful algal blooms and eutrophication: nutrient sources, composition, and consequences. *Estuaries*, *25*, 704−726.

Arnone, R. A., Martinolich, P., Gould, R. W., Sydor, M., & Stumpf, R. P. (1998). Coastal optical properties using SeaWiFS. *Ocean Optics XIV Conference, Kailua-Kona, Hawaii, 10–13 November 1998; Ocean Optics XIV CD-ROM* Washington, D.C., USA: Office of Naval Research.

Arnone, R. A., Wood, A. M., & Gould, R. W. (2004). The evolution of optical water mass classification. *Oceanography*, *17*(2), 15.

Austin, R. W. (1974). Inherent spectral radiance signatures of the ocean surface. *Ocean Color Analysis,* La Jolla. CA: Scripps Institute of Oceanography.

Babin, M., Morel, A., & Gentili, B. (1996). Remote sensing of sea surface sun-induced chlorophyll-a fluorescence: Consequences of natural variation in the optical characteristics of phytoplankton and the quantum yield of chlorophyll a fluorescence. *International Journal of Remote Sensing*, *17*, 2417−2448.

Barnes, R. A., & Zalewski, E. F. (2003). Reflectance-based calibration of SeaWiFS. II. Conversion to radiance. *Applied Optics*, *42*, 1648−1660.

Brown, C. W., & Yoder, J. A. (1994). Distribution pattern of coccolthophorid blooms in the western North Atlantic Ocean. *Continental Shelf Research*, *14*, 175−197.

Burkholder, J. M. (1998). Implications of harmful microalgae and heterotrophic dinoflagellates in management of sustainable marine fisheries. *Ecological Applications*, *8*, 37−62.

Chang, K., Kim, Y. B., Suk, M. S., & Byun, S. K. (2002). Hydrography around Dokdo. *Ocean and Polar Research*, *24*, 369−389.

Chang, F. H., Uddstrom, M., & Pinkerton, M. (2001). Studies of the winter 2000 *Gymnodinium catenatum* outbreaks in New Zealand using remotely sensed sea surface temperature and chlorophyll a data from satellites. *Proceedings of the Marine Biotoxin Science Workshop*, *Vol. 15*. (pp. 165−173). New Zealand: Wellington.

Chen, C., Zhu, J., Beardsley, R. C., & Franks, P. J. S. (2003). Physical-biological sources for dense algal blooms near the Changjiang River. *Geophysical Research Letters*, *30*, doi:10.1029/2002GL016391.

Cannizzaro, J. P., Carder, K. L., Chen, F. R., Walsh, J. J., Lee, Z., Heil, C., et al. (2002, 21–25 October). A novel optical classification technique for detection of red tides in the Gulf of Maxico; Application to the 2001–2002 bloom event. *Proceedings of the Xth International Conference on Harmful Algae* (pp. 43). Florida: St. Pete Beach.

Carder, K., & Steward, R. G. (1985). A remote sensing reflectance model of a red tide dinoflagellate off west Florida. *Limnology and Oceanography*, *30*, 286−298.

Cokacar, T., Oguz, T., & Kubilay, N. (2004). Satellite-detected early summer coccolithophore blooms and their interannual variability in the Black Sea. *Deep-Sea Research. Part 1. Oceanographic Research Papers*, *51*, 1017−1031.

Danaher, S., & Omongain, E. (1992). Singular value decomposition in multispectral radiometry. *International Journal of Remote Sensing*, *13*, 1771−1777.

Darecki, M., & Stramski, D. (2004). An evaluation of MODIS and SeaWiFS bio-optical algorithms in the Baltic Sea. *Remote Sensing of Environment*, *89*, 326−350.

EQB (Environment Quality Bulletin), Beijing, China, 2000 (in Chinese). Fu, W.C. Available from <www.people.com.cn/GB/huanbao/56/20020208/643421.html>

Falkowski, P. G., Ziemann, D., Kolber, Z., & Bienfang, P. K. (1991). Role of eddy pumping in enhancing primary production in the ocean. *Nature*, *352*, 55−58.

Fukuyo, Y., Takano, H., Chihara, M., & Matsuoka, K. (1990). Red tide organisms in Japan. *An Illustrated Taxonomic Guide* (pp. 407). Tokyo: Uchida Rokakuho, Co., Ltd.

Furuya, K., Kurita, K., & Odate, T. (1996). Distribution of phytoplankton in the East China Sea in the winter of 1993. *Journal of Oceanography*, *52*, 323−333.

Goa, Y. J. (1994). Primary productivity and phytoplankton in China Seas. In D. Zhou, Y. Liang, & C. Tseng (Eds.), *Oceanology of China Sea* (pp. 227−242). The Netherlands: Kluwer Academic Publishers.

Gao, X., & Song, J. (2005). Phytoplankton distributions and their relationship with the environment in the Changjiang Estuary, China. *Marine Pollution Bulletin*, *50*, 327−335.

Gitelson, A., Mayo, M., & Yacobi, Y. Z. (1994). Signature analysis of reflectance spectra and its application for remote observation of the phytoplankton distribution in Lake Kinneret. *International Society for Photogrammetry and Remote Sensing 6th International Symposium* (pp. 277−283). France: Val d'Isere.

Gordon, H. R., Clark, D. K., Mueller, J. L., & Hovis, W. A. (1980). Phytoplankton pigments from the Nimbus-7 Coastal Zone Color Scanner: Comparisons with surface measurements. *Science*, *210*, 63−66.

Gordon, H. R., & Morel, A. (1983). Remote assessment of ocean color for interpretation of satellite visible imagery — A review. In R. T. Barber, M. J. Bowman, C. N. K. Mooers, & B. Zetzschel (Eds.), *Lecture notes on coastal and estuarine studies* (pp. 1−144). New York: Springer-Verlag.

Hong, J. C. (2003). Ecological study on red tide in the China main estuaries and bays. Part VI. Changjiang Estuary. In Y. Z. Qi (Ed.), *China Inshore Red tide* (pp. 159−178). Beijing: Science Press.

Hooker, S.B., Firestone, E.R., & Acker, J.C. (1994). SeaWiFS Pre-launch Radiometric Calibration and Spectral Characterization. SeaWiFS technical report series, NASA Technical Memorandum 104566, Vol. 23.

Hooker, S. B., & McClain, C. R. (2000). The calibration and validation of SeaWiFS data. *Progress in Oceanography*, *45*, 427−465.

Hu, C., Carder, K. L., & Muller-Karger, F. E. (2000). Atmospheric correction of SeaWiFS imagery over turbid waters: a practical method. *Remote Sensing of Environment*, *74*, 195−206.

Hu, C., Muller-Karger, F. E., Taylor, C., Carder, K. L., Kelble, C., Johns, E., et al. (2005). Red tide detection and tracing using MODIS fluorescence data: a regional example in SW Florida coastal waters. *Remote Sensing of Environment*, *97*, 311−321.

Huang, S. (1992). *Management of Chinese estuaries* (pp. 156). Beijing: China Ocean Press.

Hyun, J. H., & Kim, K. H. (2003). Bacterial abundance and production during the unique spring phytoplankton bloom in the central Yellow Sea. *Marine Ecology Progress Series*, *252*, 77−88.

Kim, H. G., Park, J. S., & Lee, S. G. (1990). Coastal algal blooms caused by the cyst-forming dinoflagellates. *Bulletin Korean Fisheries Society*, *23*, 468−474.

Kim, H. G. (1998). Harmful algal blooms in Korean coastal waters focused on three fish killing dinoflagellates. In H. G. Lee, S. G. Lee, & C. K. Lee (Eds.), *In harmful algal blooms in Korea and China.* Pusan, Korea: NFRDI.

Kishino, M., Sugihara, S., & Okami, N. (1984). Estimation of quantum yield of chlorophyll a fluorescence from the upward irradiance spectrum in the sea. *La Mer*, *22*, 233−240.

Lee, Z. P., Carder, K. L., Steward, R. G., Peacock, T. G., Davis, C. O., & Patch, J. S. (1998). An empirical algorithm for light absorption by ocean water based on color. *Journal of Geophysical Research*, *103*, 27,967−27,978.

Lie, H. J., Cho, C. H., Lee, J. H., Niiler, P., & Hu, J. H. (1998). Separation of the Kuroshio water and its penetration onto the continental shelf west of Kyushu. *Journal of Geophysical Research*, *103*, 2963−2976.

Lie, H. J., Lee, S., Lee, J. H., Cho, C. H., & Tang, Y. (1999). Is the YSWC a persistent mean flow? *International Symposium on Progress in Coastal Engineering and Oceanography, 9–10 September, Seoul* (pp. 25−43).

Mobley, C. D. (1999). Estimation of the remote sensing reflectance from above-sea surface. *Applied Optics*, *38*, 7442−7455.

Montes-Hugo, M. A., Carder, K., Foy, R. J., Cannizzaro, J., Brown, E., & Pegau, S. (2005). Estimating phytoplankton biomass in coastal waters of Alaska using airborne remote sensing. *Remote Sensing of Environmen*, *98*, 481−493.

Morel, A., & Antoine, D. (1994). Heating rate within the upper ocean in relation to its bio-optical sate. *Journal of Physical Oceanography*, *24*, 1652−1665.

Morel, A., & Prieur, L. (1977). Analysis of variations in ocean color. *Limnology and Oceanography*, *22*, 709−722.

Olaizola, M., Ziemann, D. A., Bienfang, P. K., Walsh, W. A., & Conquest, L. D. (1993). Eddy-induced oscillations of the pycnocline affect the floristic composition and depth distribution of phytoplankton in the subtropical Pacific. *Marine Biology*, *116*, 533−542.

O'Reilly, J. E., Moritorena, S., Mitchell, B. G., Seigel, D. A., Carder, K. L., Garver, S. A., et al. (1998). Ocean color chlorophyll algorithms for SeaWiFS. *Journal of Geophysical Research*, *103*, 24,937−24,953.

Pasterkamp, R., Peters, S. W. M., Wan Der Woerd, H. J., & Hoogenboom, H. J. (2002). Detection of algal blooms in the North Sea using supervised classification of SeaWiFS reflectance imagery. *Proceeding of the International Conference on Remote Sensing for Marine and Coastal Environments, Florida, 20–22 May.*

Ruddick, K. G., Ovidio, F., & Rijkeboer, M. (2000). Atmospheric correction of SeaWiFS imagery for turbid and inland waters. *Applied Optics*, *39*, 897−913.

Sathyendranath, S. (2000). Remote sensing of ocean color in coastal and other optically complex waters. IOCCG Report, Vol. 3, Dartmouth, Nova Scotia, IOCCG Project Office, pp. 140.

Sarangi, R. K., Chauhan, P., & Nayak, S. R. (2004). Detection and monitoring of *Trichodesmium* bloom in the coastal waters off Saurashtra coast, India using IRS-P4 OCM data. *Current Science*, *86*, 1636−1641.

Shen, Z., Lu, J., Liu, X., & Diao, H. (1992). Distribution characteristics of the nutrients in the Changjiang River estuary and the effect of the Three Gorges Project on it. *Studia Marina Sinica*, *39*, 109−129.

Shumway, S. E. (1990). A review of the effects of algal blooms on shellfish and aquaculture. *Journal of World Aquaculture Society*, *21*, 65−104.

Siegel, D. A., Wang, M., Maritorena, S., & Robinson, W. (2000). Atmospheric correction of satellite ocean color imagery: the black pixel assumption. *Applied Optics*, *39*, 3582−3591.

Steidinger, K. A., & Haddad, K. D. (1981). Biologic and hydrographic aspects of red tides. *Bioscience*, *31*, 814−819.

Stumpf, R. P. (2001). Applications of satellite ocean color sensors for monitoring and predicting harmful algal blooms. *Journal of Human and Ecological Risk Assessment*, *7*, 1363−1368.

Stumpf, R. P., Culver, M. E., Tester, P. A., Tomlinson, M., Kirkpatrick, G. J., Pederson, B. A., et al. (2003). Monitoring *Karenia brevis* blooms in the Gulf of Mexico using satellite ocean color imagery and other data. *Harmful Algae News*, *2*, 147−160.

Stumpf, R. P., & Pennock, J. R. (1991). Remote estimation of the diffuse attenuation coefficient in a moderately turbid estuary. *Remote Sensing of Environment*, *38*, 182−191.

Subramaniam, A., Brown, C. W., Hood, R. R., Carpenter, E. J., & Capone, D. G. (2002). Detecting *Trichodesmium* blooms in SeaWiFS imagery. *Deep-Sea Research. Part 2. Topical Studies in Oceanography*, *49*, 107−121.

Subramaniam, A., & Carpenter, E. J. (1994). An empirically derived protocol for the detection of blooms of the marine cynobacterium *Trichodesmium* using CZCS imagery. *International Journal of Remote Sensing*, *15*, 1559−1569.

Suh, Y. S., Jang, L. H., Lee, N. K., & Ishizaka, J. (2004). Feasibility of red tide detection around Korean waters using satellite remote sensing. *Journal of Fisheries Science and Technology*, *7*, 148−162.

Tang, D. L., Kawamura, H., Oh, I. S., & Baker, J. (2006). Satellite evidence of harmful algal blooms and related oceanographic features in the Bohai Sea during autumn 1998. *Advances in Space Research*, *37*, 681−689.

Tang, D. L., Kester, D. R., Ni, I. H., Qi, Y. Z., & Kawamura, H. (2003). In-situ and satellite observations of a harmful algal bloom and water condition at the Pearl River estuary in late autumn 1998. *Harmful Algae News*, *2*, 89−99.

Tomlinson, M. C., Stumpf, R. P., Ransibrahmanakul, V., Truby, E. W., Kirkpatrick, G. J., Pederson, B. A., et al. (2004). Evaluation of the use of SeaWiFS imagery for detecting *Karenia brevis* harmful algal blooms in the eastern Gulf of Mexico. *Remote Sensing of Environment*, *91*, 293−303.

Wei, H., Sun, J., Moll, A., & Zhao, L. (2004). Phytoplankton dynamics in the Bohai Sea — observations and modeling. *Journal of Marine Systems*, *44*, 233−251.

Yuki, K., & Yoshimatsu, S. (1989). Two fish-killing species of *Cochlodinium* from Harima-Nada, Seto Inland Sea, Japan. In T. Okaichi, D. Anderson, & T. Nemoto (Eds.), *Red Tides: Biology, Environmental Science, and Toxicology* (pp. 451−454). New York: Elsevier.

Zabicki, K. E. (1995). Determining the existence of cyanobacterial blooms using CZCS imagery, student report, NASA/Univ of Md. Summer Fellowship Program in Remote Sensing of the Oceans, Greenbelt, Md.

Zhang, J., Hang, W., & Liu, M. (1994). Geochemistry of major Chinese river-estuary systems. In D. Zhou, Y. Liang, & C. Tseng (Eds.), *Oceanology of China Sea* (pp. 179−188). The Netherlands: Kluwer Academic Publishers.